

1 Developing Functional Recharge Systems to Control Saltwater 2 Intrusion via Integrating Physical, Numerical, and Decision-Making 3 Models for Coastal Aquifer Sustainability

4 Yehia Miky¹, Usama Hamed Issa^{2,3}, Wael Elham Mahmod^{3,4}

5 ¹Department of Geomatics, Faculty of Architecture and planning, King Abdulaziz University, Jeddah, Saudi Arabia;
6 yhhassan@kau.edu.sa

7 ²Department of civil engineering, Faculty of Engineering, Minia University, Egypt; usama.issa@mu.edu.eg

8 ³Department of civil engineering, college of Engineering, Taif University, Saudi Arabia; wemahmod@tu.edu.sa;
9 +966543656209

10 ⁴Civil Engineering Department, Faculty of Engineering, Assiut University, 71515 Assiut, Egypt; wdpp2006@aun.edu.eg; +20-
11 01006328492,
12 orcid.org/0000-0003-4340-0525

13 *Correspondence to:* Wael Elham Mahmod (wdpp2006@aun.edu.eg)

14 **Abstract.** Controlling the hydraulic heads along the coastal aquifer may help to effectively manage saltwater intrusion,
15 improve the conventional barrier's countermeasure, and ensure the coastal aquifer's long-term viability. This study proposed a
16 framework that utilizes a decision-making model (DMM) by incorporating the results of two other models (physical and
17 numerical) to determine proper countermeasure components. The physical model is developed to analyze the behavior of
18 saltwater intrusion in unconfined coastal aquifers by conducting two experiments: one for the base case and one for the
19 traditional vertical barrier. MODFLOW is used to create a numerical model for the same aquifer, and experimental data is
20 used to calibrate and validate it. Three countermeasure combinations, including vertical barrier, surface, and subsurface
21 recharges, are numerically investigated using three model case categories. Category (a) model cases investigate the hydraulic
22 head's variation along the aquifer to determine the best recharge location. Under categories (b) and (c), the effects of surface
23 and subsurface recharges are studied separately or in conjunction with a vertical barrier. As a pre-set of the DMM, evaluation
24 and classification ratios are created from the physical and numerical models, respectively. The evaluation ratios are used to
25 characterize the model cases results, while the classification ratios are used to classify each model case as best or worst. An
26 analytic hierarchy process (AHP) as DMM is built using the hydraulic head, salt line, repulsion, wedge area, and recharge as
27 selection criteria to select the overall best model case. According to the results, the optimum recharging location is in the length
28 ratio (LR) from 0.45 to 0.55. Furthermore, the DMM supports case3b (vertical barrier + surface recharge) as the best model
29 case to use, with a support percentage of 47.93%, implying that this case has a good numerical model classification with a
30 maximum repulsion ratio (Rr) of 29.4%, and an acceptable wedge area ratio (WAR) of 1.25. The proposed framework could
31 be used in various case studies under different conditions to assist decision-makers in evaluating and controlling saltwater
32 intrusion in coastal aquifers.

33 **Keywords:** Saltwater intrusion · Hydraulic heads · Unconfined coastal aquifer · Vertical barrier · Surface recharge · subsurface
34 recharge · Decision making · AHP

35 1 Introduction

36 Due to the natural effects of long-term climate change, such as sea level change and tidal intensity fluctuations, seawater flows
37 toward the freshwater aquifers. In addition, increased water demands accompanied by anthropogenic activities such as
38 excessive pumping of freshwater in coastal areas cause the lowering of water tables as well as saltwater intrusion (Abd-Elaty
39 et al. 2019; Sutar and Rotte 2022). Saltwater intrusion lowers the availability and quality of freshwater in coastal regions, as
40 reported at many locations all over the world (Qi and Qiu 2011; Shi and Jiao 2014; Anders et al. 2014; Cary et al. 2015;

41 Srinivasamoorthy 2015; Abd-Elhamid 2016; Eissa et al. 2018; Abd-Elhamid et al. 2019; Pramada et al. 2021). Therefore, it is
42 important to control saltwater intrusion with efficient countermeasures to achieve sustainable freshwater sources.

43 Traditional methods for controlling saltwater intrusion include reducing pumping rates, relocating pumping wells, changing
44 pumping patterns, constructing physical subsurface barriers, and saltwater abstraction (Abd-Elhamid and Javadi 2011;
45 Kallioras et al. 2013; Cai et al. 2015; Huang and Chiu 2018; Abd-Elhamid et al. 2019; Hussain et al. 2019). The limitations
46 and high costs of the aforementioned methods pose substantial challenges to their implementation.

47 Artificial recharge techniques can be used for establishing hydraulic barriers to mitigate saltwater intrusion while recovering
48 SGD (Raja Shekar and Mathew, 2023; Salehi Shafa et al., 2023; Wadi et al., 2022). These techniques have several advantages
49 compared to traditional methods, including low cost, no inundation storage space, less water evaporation, and improved water
50 quality (Ríos et al., 2023). Although artificial recharge has numerous advantages, it also has disadvantages, including
51 groundwater contamination from surface water, difficulty in implementation due to a lack of understanding of aquifer
52 hydrogeological properties, the potential for environmental damage and soil disturbance, and high maintenance costs (Hasan
53 et al., 2019). Surface recharge systems include ditches and furrows, recharge basins, stream augmentation, and runoff
54 conservation structures (terracing, contour bunds, percolation tanks, gully plugs, Nalah bunds, and check dams) (Maliva 2020b,
55 c; ASCE 2001). On the other hand, subsurface recharge systems include subsurface injection wells, borewells, and recharging
56 pits and shafts (Maliva 2020a, d; ASCE 2001). Combining traditional and artificial recharge techniques is one way to overcome
57 the disadvantages of both. Although many studies investigate saltwater intrusion in coastal aquifers, only a limited number
58 study the control methods of saltwater intrusion (Robinson et al., 2016; Panthi et al., 2022).

59 Physical and numerical models have not only proven to be more effective tools for selecting the optimum solutions for
60 controlling saltwater intrusion but can also be used to reduce the need for expensive hydrogeological and environmental
61 investigations before constructing a full-scale project (Mantoglou 2003; Zhou, et al. 2003; Abarca et al. 2006; Sutherland and
62 Barfuss, 2011; Singh 2015; Abd-Elaty et al. 2019; Guo et al. 2019; M Armanuos et al. 2019).

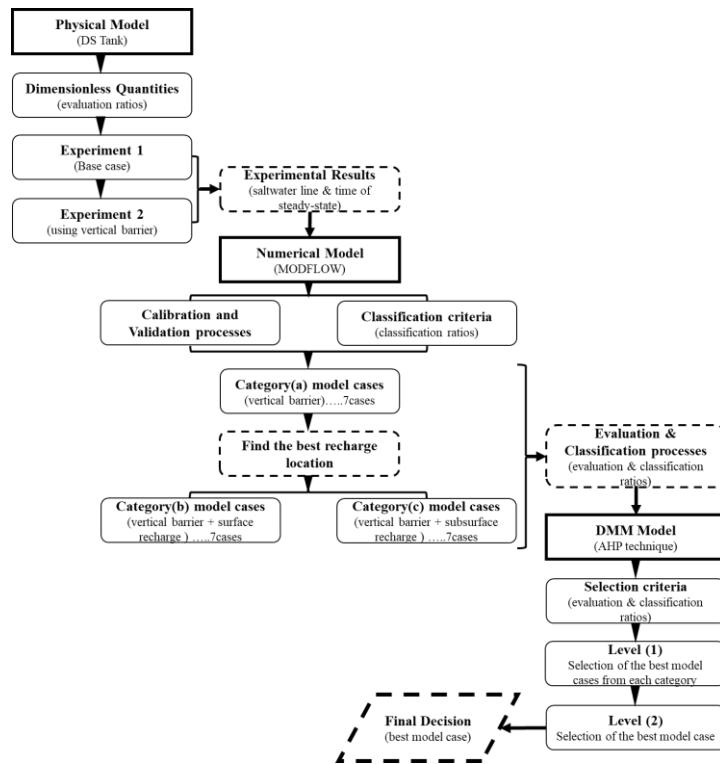
63 Although physical and numerical models are useful in determining the optimum solutions for controlling saltwater intrusion,
64 deficiencies in the acquisition of appropriate evidence to support the final decision are discovered. Since the scenarios of
65 hydrogeological models for a specific aquifer cannot agree on minimizing intrusion, improving groundwater availability, being
66 environmentally friendly, and being cost-effective. It is necessary to use decision models in conjunction with physical and
67 numerical models to guide stakeholders toward sustainable resource management based on a set of criteria. The analytical
68 hierarchy process (AHP) is a decision-making method that has been used alone or in conjunction with other techniques such
69 as GIS and fuzzy logic in a variety of groundwater-related fields. Based on a broader set of criteria, this technique is used to
70 guide stakeholders involved in groundwater development and sustainable resource management (Vaidya and Kumar 2006;
71 Alwetaishi et al. 2017). The applications of AHP in the field of groundwater include assessing groundwater vulnerability by
72 developing indices based on hydrogeological parameters and mapping groundwater potential zones (Arunbose et al. 2021;
73 Osiakwan et al. 2022; Ahmadi et al. 2021; Castillo et al. 2022; Achu et al. 2020; Sajil Kumar et al. 2022; Nithya et al. 2019;
74 Phin et al., 2022; Zghibi et al., 2020; (Mallick et al., 2019) (Shao et al., 2020). In the field of saltwater intrusion, a GIS-based
75 AHP weighted index overlay analysis technique has been demonstrated to determine the distribution of groundwater
76 vulnerability (Gangadharan, Nila, et al. 2016; Güllü and Kavurmacı 2023). A fuzzy-AHP evaluation model is developed for
77 analyzing the level of seawater intrusion in long-term monitoring data from multiple river basins (Yang et al., 2022). The AHP
78 is also used to compute weights for the GALDIT parameters, which are used to assess the vulnerability of coastal aquifers to
79 saltwater intrusion (Pham et al., 2022).

80 According to the preceding overview, both traditional and artificial techniques of controlling seawater intrusion have
81 limitations, and using physical, numerical, and decision-making models is crucial. The unconfined coastal aquifer is
82 investigated in this study, and physical, numerical, and decision-making models are utilized to investigate surface and
83 subsurface recharge methods, either alone or in combination with typical vertical barriers. On the other hand, the behaviors of

84 saltwater intrusion, groundwater flow, and hydraulic head are numerically investigated using three categories of model cases:
85 categories (a), (b), and (c). Category (a) model cases explore the variation of hydraulic head along the aquifer in order to
86 determine the appropriate recharging location. The impacts of surface and subsurface recharges are explored separately or in
87 conjunction with a vertical barrier in categories (b) and (c). The aims of this study are: (i) to examine experimentally the
88 behavior of saltwater intrusion via coastal unconfined aquifers with and without vertical barrier countermeasures; (ii) to
89 develop a validated numerical model regarding the experimental findings of transitory saltwater intrusion; (iii) to identify the
90 optimal recharging location utilizing the location of the minimum hydraulic head; (v) to determine the optimal vertical barrier
91 depth for saltwater intrusion management; (iv) to identify the components of an effective countermeasure system, such as a
92 vertical barrier, surface recharge, and subsurface recharge, either alone or in combination; (vi) to develop a DMM model to
93 aid decision makers in the selection among several saltwater countermeasures and picking the most appropriate one depending
94 on various demanding scenarios.

95 **2 Materials and Methodologies**

96 Saltwater intrusion is investigated experimentally in this study by developing a laboratory physical model of an unconfined
97 coastal aquifer. Two experiments are carried out in this part, and dimensionless quantities are formed, namely evaluation ratios.
98 These evaluation ratios are used to analyze and characterize the saltwater line and hydraulic head variations of the numerical
99 model cases, as forthcoming later. A numerical finite difference model is created, and the validation and calibration processes
100 are carried out using the experimental results. Following that, numerical methods are utilized to investigate how to control
101 saltwater intrusion, taking into account the combined effect of using vertical barriers with surface or subsurface recharge
102 systems, as demonstrated by model cases divided into three categories (a, b, and c), each with seven cases. Category (a) model
103 cases are used to determine the location of the minimal hydraulic heads, which are suggested to be the locations of the indicated
104 artificial recharge systems. Categories (b) and (c) investigate the impacts of surface and subsurface recharges on saltwater
105 intrusion at the indicated locations, either alone or in conjunction with a vertical barrier. A classification process is then
106 implemented to classify model cases in each category as the best or worst model case using a developed set of ratios, namely
107 classification ratios. Because each model case is expected to have benefits and drawbacks, as well as several criteria governing
108 the model cases, the benefits and drawbacks of each model case should be quantified in order to identify the most effective
109 one. Following that, the most effective model case is decided on using a new DMM model based on the AHP technique. To
110 make the final decision, two selection levels (levels 1 and 2) are considered. Level 1 is used to select the best model case from
111 each category (three model cases). While level 2 is utilized for selecting the best overall model case. **Figure 1** illustrates a
112 flow chart for the framework of the study.



113

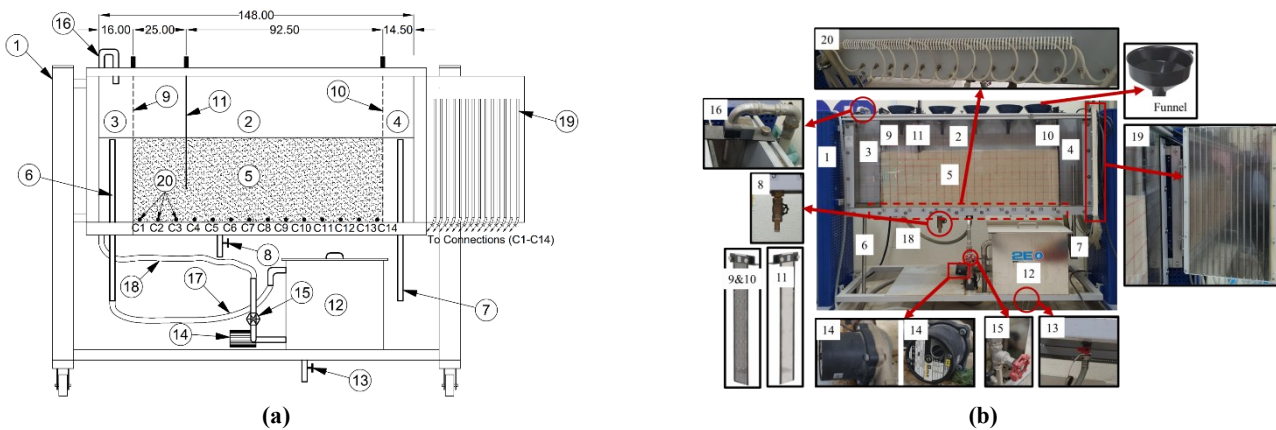
114 **Figure 1: Flow chart shows the proposed framework to identify most effective model case using the physical, numerical, and decision-**
 115 **making models**

116 **2.1 Experimental Setup**

117 **2.1.1 Drainage and Seepage Tank (DS tank)**

118 The DS Tank is used in this study to visualize groundwater flow through permeable porous media. The model of the DS tank
 119 that is used in the current study is HM 169 GUNT HAMBURG (G.U.N.T, 2023). The DS tank consists of a porous media
 120 container, a lower water tank as a water source, a pump for the water flow, a valve to adjust the water supply, and measuring
 121 connections in the experiment section, which are connected to 14 glass tube manometers to display and measure hydraulic
 122 heads along the DS Tank. The sand container consists of an aluminum rectangular tank with a transparent front side
 123 (methacrylate material) to visualize groundwater flow and optimize observation of the experiments through the porous media.
 124 In the DS Tank, two fine mesh screens are used to create feed and discharge chambers and to separate the experimental section
 125 from these two chambers. There are two adjustable overflow pipes in the DS Tank for adjusting the water levels in the
 126 mentioned chambers and measuring the water flow. To prevent seawater intrusion, an aluminum sheet pile is used as a vertical
 127 barrier. As a result, the DS Tank has a closed water circuit with a storage tank and pump. The DS Tank and its components
 128 are depicted in **Figure 2 and Table 1**.

129
 130



131 **Figure 2: DS Tank and its components: (a) Drawing of details, (b) Photo**

132 **Table 1: DS Tank components and descriptions**

No.	Component Name	Description	No.	Component Name	Description
1	Steel frame	The DS Tank's frame	11	Vertical aluminum sheet pile	Vertical barrier to control saltwater intrusion
2	Experimental section	Tank with porous media for monitoring saltwater intrusion	12	Storage tank	The primary source of seawater
3	Feed Chamber	Source of saltwater	13	Draining pipe2	Before the next experiment, drain the saltwater from the storage tank.
4	Discharge Chamber	Source of freshwater	14	Pump	Pumping saltwater to the feed chamber
5	Porous media	Silica sand (0.71-1.18mm)	15	Pump valve	Pump flow rate adjustment
6	Outflow pipe1	Changing the saltwater level in the feed chamber	16	Saltwater inflow pipe	Connecting with a pump to allow saltwater to flow from the pump to the feed chamber
7	Outflow pipe2	Changing the level of freshwater in the discharge chamber	17	Hose1	Connecting the outflow pipe 1 to the storage tank
8	Draining pipe1	Before beginning a new experiment, drain the water from the experimental section.	18	Hose2	Linking the saltwater inflow pipe to the pump
9	Vertical screen1	Separating the feed chamber from the experimental section	19	14 glass manometer tubes	Hydraulic head monitoring along the experimental section
10	Vertical screen2	Separating the discharge chamber from the experimental section	20	Measuring connections	linked to the 14 glass manometer tubes

133 **2.1.2 Configuration and Experimental Set**

134 The DS tank and the associated materials, including saltwater, freshwater, and porous media, are pre-set for the experiments.

135 A horizontal and vertical scale of 5cm x 5cm is drawn on the transparent front side of the DS tank, as shown in **Figure 3**. The

136 left chamber is configured as a saltwater feed chamber with a width of 16cm. The right chamber is configured as a freshwater

137 discharge chamber with a width of 14.5cm. Vertical screen barriers separate the experimental section of the DS tank (length

138 117.5cm) from the feed and discharge chambers. The experimental section is filled to a depth of 40cm with porous media soil

139 (graded silica sand with grain sizes ranging from 0.71 to 1.18mm (see **Figure 3**). The filling process is done in layers of 5cm

140 each, with a falling height of 50 cm for each layer, to ensure a homogeneous hydrogeological property of the media sand. In

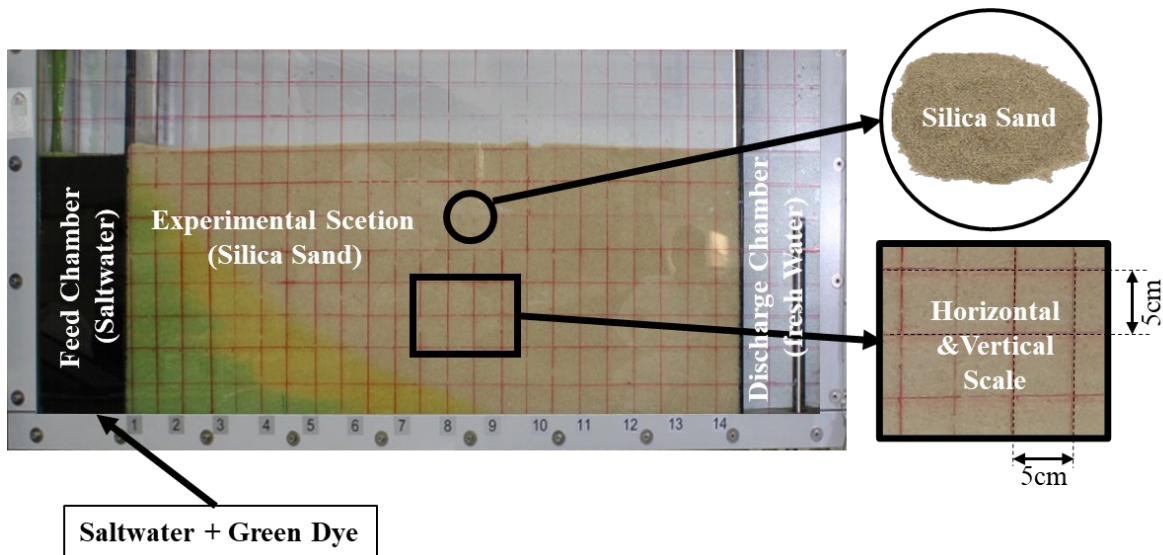
141 the filling process, funnels are used, which are distributed along the experimental section as shown in **Figure 1b**.

142 The seawater used in the experiments is collected from the Red Sea, and its density, as well as that of the freshwater, is

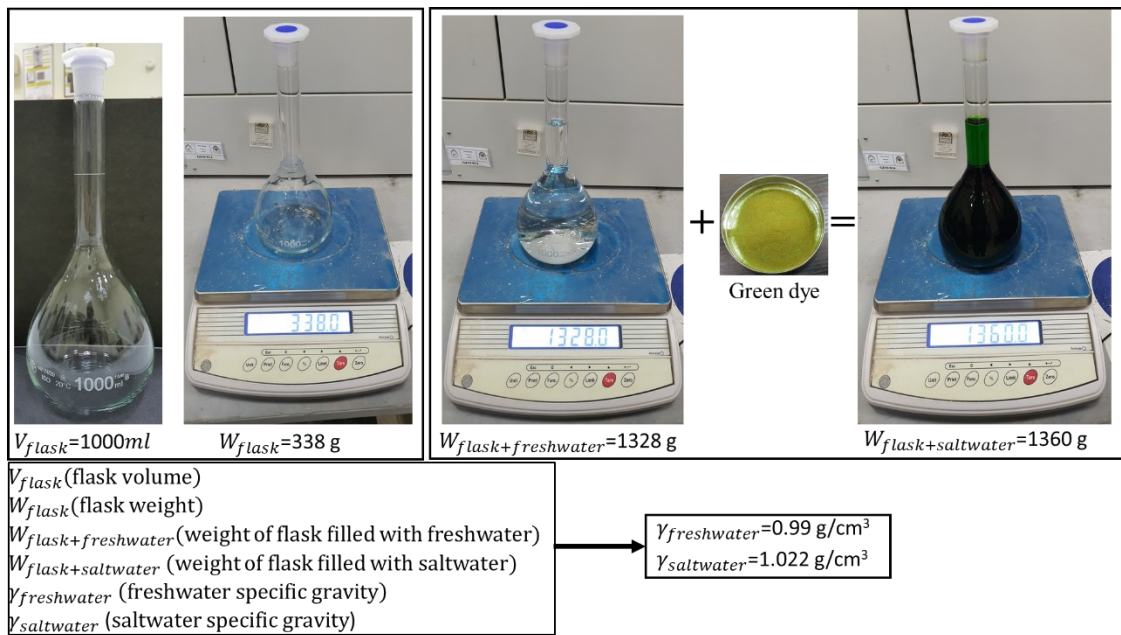
143 calibrated using a sensitive scale and a standard flask (see **Figure 4**). According to the calibration, the densities of saltwater

144 and freshwater are 0.99 and 1.022 g/cm³, respectively. In saltwater, a 0.15 g/L concentration of green food dye is used to easily

145 visualize the saltwater line and measure the intrusion distance inside the media sand (see **Figure 3**).



146
147 **Figure 3: DS Tank pre-set for experimental procedures**



148
149 **Figure 4: Saltwater and freshwater calibration**

150 **2.1.3 Experimental Procedures**

151 The experiment procedures include the following five steps:

152 1-Freshwater saturation of the media sand: at the start of the experiment, the outflow pipes 1 and 2 for both the feed and
153 discharge chambers are set to be at the same level as the media sand surface (40 cm from the DS Tank bed). Following that,
154 fresh water is discharged at a constant rate into both chambers until the media sand in the experimental section is saturated.
155 The hydraulic heads along the experimental section are monitored by the 14 glass tube manometers until the water level reaches
156 the sand surface in all the manometers to verify the saturation condition.

157 2-Feeding the experiment with colored saltwater: in the feed chamber, an aluminum sheet pile is used to block water seepage
158 through the experimental section. Following that, the feed chamber's outflow pipe 1 is moved to the DS Tank bed level to
159 empty it of freshwater. The outflow pipe is then returned to its previous level (media sand surface level), and the storage tank
160 is subsequently emptied and filled with the green-dyed saltwater. When the pump is turned on and the pump valve is opened,
161 saltwater begins to fill the feed chamber all the way to the top of the outflow pipe1. Following that, the pump valve is manually
162 adjusted to maintain the saltwater level at the surface of the media sand.

163 3-Adjusting the water levels in the feed and discharge chambers: the first step in this process is to remove the aluminum sheet
 164 pile from the feed chamber. Furthermore, to achieve a suitable flow through the media sand, the difference in water levels
 165 between the feed and discharge chambers is tested several times and finally adjusted to 10 cm, resulting in a hydraulic gradient
 166 of 0.085. To accomplish this, the outflow pipe 2 for the discharge chamber is adjusted to be 10 cm below the media sand
 167 surface.

168 4-Monitoring of saltwater intrusion: in the experimental section, saltwater begins to infiltrate through the media sand and can
 169 be observed through the transparent front side of the DS Tank. The temporal saltwater intrusion could be measured using the
 170 horizontal and vertical scales drawn on the transparent front side. The saltwater intrusion is measured at 30-minute intervals.
 171 Photos for each time interval are taken with a high-resolution digital camera and used to validate the observed saltwater lines
 172 with AutoCAD software. During the experiment, the freshwater level inside the discharge chamber rises until it reaches its
 173 maximum level by adjusting the outflow pipe2 level above the media sand surface level until it reaches a steady state.

174 This experimental part of the study considers two experiments:

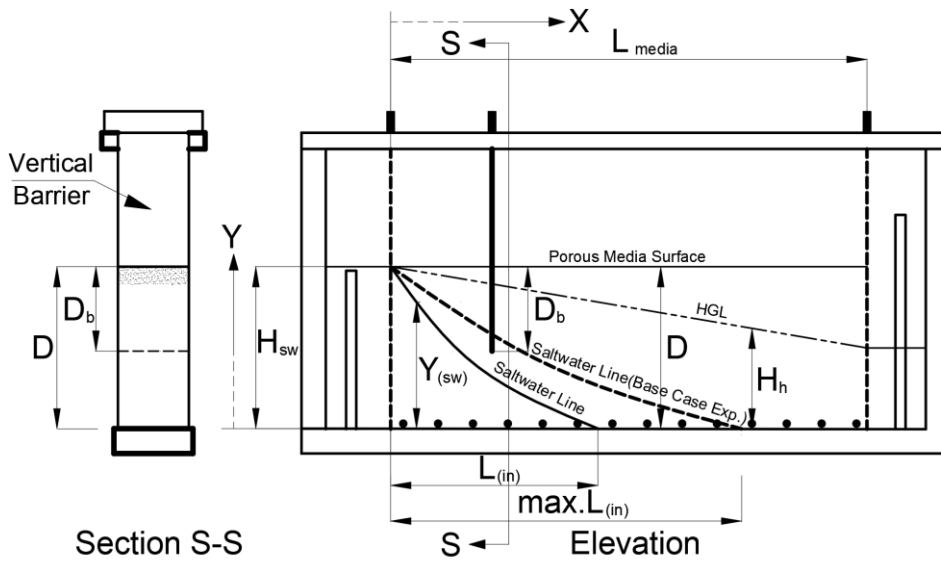
175 Experiment 1 (Base Case): this is the case in which the saltwater intrusion through the media sand is studied without any
 176 countermeasures. In this case, the procedures from steps 1 to 4 are carried out.

177 Experiment 2 (using a vertical barrier): through this experiment, the media sand is removed from the experimental section.
 178 Then, the vertical aluminum sheet pile (vertical barrier) is used as a countermeasure against saltwater intrusion and placed in
 179 the experimental section, 25cm from the feed chamber. Hereafter, media sand is refilled in the experimental section. The
 180 penetration depth of the vertical aluminum sheet pile is set below the silica sand surface by a depth of 30cm. Then, the steps
 181 from 1 to 4 are implemented.

182 2.2 Evaluation Ratios

183 Based on the geometry and experiment design given in the preceding section, **Figure 5** and **Table 2** list variables, parameters,
 184 and constants that affect saltwater intrusion. Following that, three dimensionless quantities are proposed for evaluating the
 185 results (see **Table 3**):

- 186 (1) Three variables, namely evaluation ratios, will be used to analyze the output results.
- 187 (2) One parameter that operates as experimental run constraints is referred to as a conditional parameter.
- 188 (3) Two geometric parameters are used to assign the hydraulic gradient and saltwater profile.



189
 190 **Figure 5: Geometric characteristics of the experiments**

191
 192

No.	Quantity	Type			Definition
		Constant	Parameter	Variable	
1	H_{sw}	√			Hydraulic Head of the saltwater boundary
2	D	√			Sand media depth
3	L_{media}	√			Sand media length (experimental section length)
4	$max.L_{(in)}$	√			Maximum length of saltwater intrusion (attained for experiment 1 (base case))
5	D_b		√		Vertical barrier depth
6	X			√	Horizontal distance from the saltwater boundary measured for any embedded point in the media sand
7	Y			√	Vertical distance measured from the experimental section bed for any embedded point in the media sand
8	$Y_{(sw)}$			√	Observed saltwater intrusion depth at any X distance at a specific time (t).
9	H_h			√	Observed hydraulic head at any X distance at a specific time (t).
10	$L_{(in)}$			√	The observed length of saltwater intrusion at a specific time (t)

194 Taking into account the characteristics listed in **Table 2**, the dimensionless quantities that will be used in this study as
 195 evaluation ratios, conditional, and geometric parameters for examining the output findings are presented in **Table 3**.

196 **Table 3: Suggested evaluation ratios, conditional parameters and geometric parameters**

	Quantities	Definition (Abbreviation)	Physical meaning
Evaluation Ratios	$L_{(in)}/max.L_{(in)}$	Intrusion Ratio (IR)	Variation of intrusion length over time (t) with reference to the maximum intrusion length (base case)
	$Y_{(sw)}/H_{sw}$	Salt Line Ratio (SLR)	A function demonstrates the variation in intrusion depth as a function of distance X and time (t) due to saltwater boundary head. In the comparative analysis of the results, the average SLR value (SLR _{avg}) will be used.
	H_h/H_{sw}	Hydraulic Head Ratio (HHR)	A function demonstrates the variation of the hydraulic head due to the influence of the saltwater boundary head at a particular distance X and time (t). In the comparative analysis of the results, the minimum value of HHR and its location will be taken into account.
Conditional Parameter	D_b/H_{sw}	Barrier Depth Ratio (BDR)	The ratio of barrier depth to saltwater boundary head depth. This ratio operates as an experimental run constraint.
Geometric Parameters	X/L_{media}	Length Ratio (LR)	The horizontal distance X for a certain location in the experimental section to the length of the sand media.
	Y/D	Depth Ratio (DR)	The vertical distance Y for a certain location in the experimental section to the total media sand depth.

197 2.3 Conceptual Model

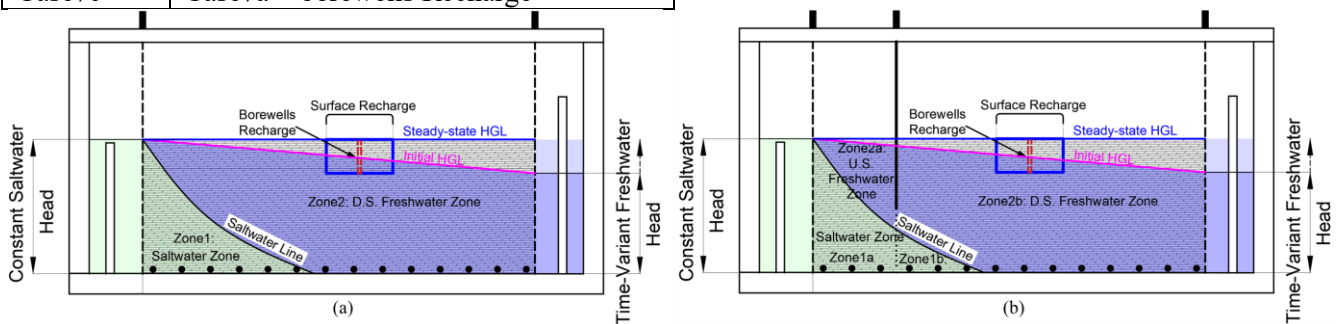
198 A proper conceptual model could be provided as a pre-set for developing a numerical model based on the experimental set and
 199 procedures previously presented in sections 2.1 and 2.2. The numerical investigation of saltwater intrusion will be conducted
 200 using either a traditional vertical barrier or artificial recharge approaches. To control seawater intrusion using a vertical barrier,
 201 various penetration depths will be simulated. Surface and subsurface recharge systems will be used as artificial recharge
 202 methods. To determine their effectiveness in controlling the saltwater intrusion problem, each of the management techniques
 203 is evaluated independently and in combination with vertical barrier. Error! Reference source not found. shows the numerical
 204 model cases being explored under different constraints. The suggested conceptual system is presented in **Figure 6**, taking into

205 account the boundary heads, initial hydraulic grade line (HGL), barrier depth and location, and artificial recharge methods.
 206 When there is no vertical barrier, two water zones can be identified: zone 1 (saltwater zone) and zone 2 (freshwater zone), as
 207 shown in **Figure 6a**. After using a vertical barrier, zones 1 and 2 are further partitioned into two zones: zone 1a and zone 1b
 208 for saltwater and zone 2a and zone 2b for freshwater, as shown in **Figure 6b**. The key features of the conceptual system are
 209 outlined below.

- 210 1. A constant-head saltwater boundary.
- 211 2. A time-variant head freshwater boundary that advances from the initial head to equilibrium with the saltwater boundary in
 212 the steady-state condition.
- 213 3. A vertical barrier of variable depths at a certain location.
- 214 4. A source of surface and subsurface artificial recharge.

215 **Table 4: The studied cases using numerical simulation**

Category (a): using vertical barrier	
Model Cases	Description
Case1a	Base Case (Verification of experiment1)
Case2a	$BDR=0.875$
Case3a	$BDR=0.75$ (Verification of experiment2)
Case4a	$BDR=0.625$
Case5a	$BDR=0.50$
Case6a	$BDR=0.375$
Case7a	$BDR=0.125$
Category (b): using vertical barrier and surface recharge	
Model Cases	Conditional Parameters
Case1b	Case1a + Surface Recharge
Case2b	Case2a + Surface Recharge
Case3b	Case3a + Surface Recharge
Case4b	Case4a + Surface Recharge
Case5b	Case5a + Surface Recharge
Case6b	Case6a + Surface Recharge
Case7b	Case7a + Surface Recharge
Category (c): using vertical barrier and subsurface recharge	
Model Cases	Conditional Parameters
Case1c	Case1a + borewells Recharge
Case2c	Case2a + borewells Recharge
Case3c	Case3a + borewells Recharge
Case4c	Case4a + borewells Recharge
Case5c	Case5a + borewells Recharge
Case6c	Case6a + borewells Recharge
Case7c	Case7a + borewells Recharge



216

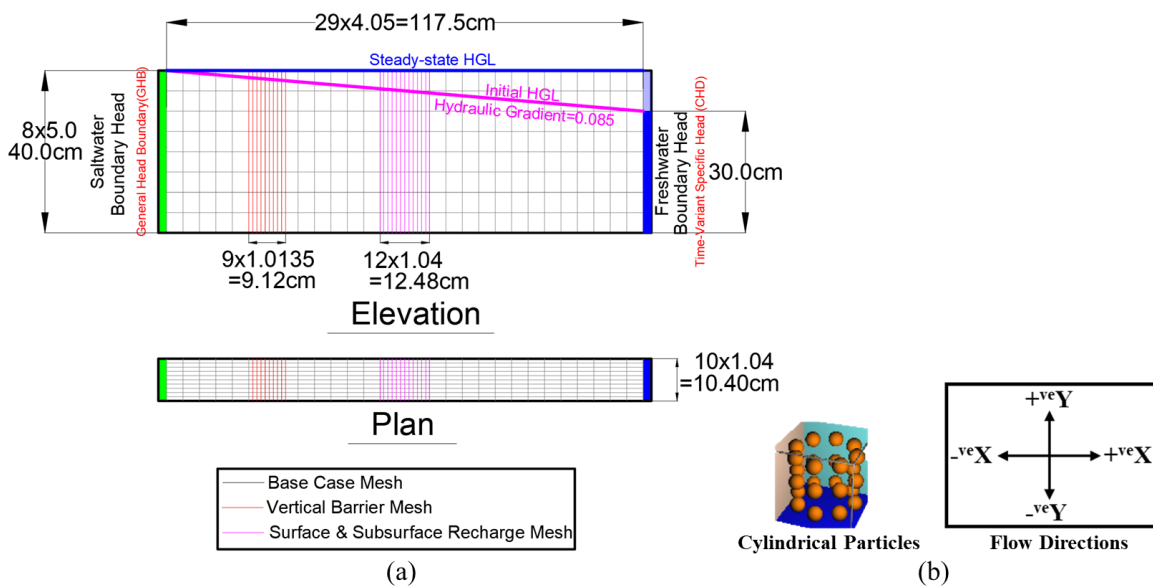
217 **Figure 6: Saltwater intrusion conceptual model: (a) freshwater and saltwater zones without barrier, (b) freshwater and saltwater**
 218 **zones with barrier**

219 **2.4 Numerical Model Development**

220 MODFLOW-2005, in conjunction with the SWI2 package, is used in this study for numerical modeling of saltwater
 221 intrusion(Harbaugh, 2005). SWI2 is a software package used to analyze three-dimensional groundwater flow, model saltwater
 222 intrusion, and calculate hydraulic heads(Bakker et al., 2013). The main advantage of using the SWI2 package is that it requires
 223 fewer cells for the simulation process than variable-density groundwater flow packages like SEAWAT. The ability of SWI2
 224 to represent each aquifer as a single layer of cells results in significant model run-time savings.

225 MODPATH is a post-processing package for particle tracking that computes and displays three-dimensional pathlines based
 226 on MODFLOW output (Pollock, 2016). The MODPATH packages are used to visualize the flow behavior of both freshwater
 227 and saltwater through the sand media by visualizing the expert transport trajectories coming from the saltwater boundary, the
 228 freshwater boundary, and the flow path from the recharge area for the cases defined in Error! Reference source not found.. The
 229 particle tracking in the MODPATH package is simulated in the forward tracking direction using cylinder particle placement,
 230 as illustrated in **Figure 7b**.

231 On the basis of the conceptual model, the saltwater boundary cells are represented by the General-Head Boundary (GHB)
 232 package. The Time-Variant Specified-Head (CHD) package is applied to the model freshwater boundary cells to obtain the
 233 same results as the experiments, with an initial hydraulic gradient of 0.085. The recharge value for each recharge type will be
 234 relevant to the flow across the saltwater boundary for each model case b, with the constraint that the hydraulic heads do not
 235 exceed the medium sand level as a maximum value. Various discretization systems are also examined in order to provide an
 236 accurate assessment of discrepancies in head drawdowns and water balances. In this study, 8 model layers with 2320 cell
 237 discretization are used, as shown in Figure 7a. Furthermore, as shown in Figure 7b, the flow direction will be characterized as
 238 $+veY$, $-veY$, $+veX$, and $-veX$.



239 (a)
 240 **Figure 7: Structure of the numerical model: (a) discretization and boundary conditions, (b) particle tracking and flow directions**

241 **2.4.1 Calibration and Verification Processes**

242 Many factors contribute to groundwater model inconsistency, including hydrogeological properties, discretization, potentially
 243 spatial discretization, time step, and solver parameters. Using the experimental results, many trials are carried out to calibrate
 244 the model using various hydrogeological properties, with reference to (Domenico et al. 1998; Rotz 2021). The transient stress
 245 period, on the other hand, will be assigned to be more than that needed for the experiment, with a proper equal interval time

246 step. The impact on the heads on the cells and the accumulated volume water balance are evaluated. Following that, a
247 verification procedure is implemented for:

248 1- Confirming the time when a steady-state condition occurs in based the results of experiment 1.

249 2- Fitting the observed saltwater line in experiments 1 and 2 for the transient and steady-state conditions.

250 2.4.2 Classification Ratios

251 As a starting point for selecting the best model case for controlling saltwater intrusion, four ratios are suggested to classify the
252 model cases included in categories (a), (b), and (c). These ratios are calculated using the numerical results of the models. Each
253 ratio is calculated for each model case and then classified by its value into best or worst. These ratios are the increase of
254 saltwater ratio (SLR_i), repulsion ratio (R_r), wedge area ratio (WAR), and recharge ratio (RER). The four ratios are computed
255 using the equations 1, 2, 3, and 4, respectively, with the RER ratio computed only for cases in categories (b) and (c). The
256 criteria for classifying the best model cases are that they have low values of SLR_i , WAR, and RER, as well as the maximum
257 value of R_r . On the other hand, cases with high values of SLR_i , WAR, and RER, as well as the lowest value of R_r , are classified
258 as the worst model cases and are not recommended for controlling saltwater intrusion. Because of the difficulty of having a
259 model case have all the best or worst values of classification ratios to be classified as the best or worst model case (unclassified
260 model case), it is important to use the DMM models to use the values of these classification ratios to make the final decision.

$$261 \quad SLR_i = SLR_{avg}^{case\ k} - SLR_{avg}^{case1a} \quad (1)$$

$$262 \quad R_r = IR_{case1a} - IR_{casek} \quad (2)$$

$$263 \quad WAR = \frac{Wedge\ Area_{case(k)}}{Wedge\ Area_{case1a}} \quad (3)$$

$$264 \quad RER = \frac{Recharge_{case(j)}}{Saltwater\ boundary\ Recharge_{case(j)}} \quad (4)$$

265 Where case(k) is any case included at any category (a, b, and c), and case(j) is the cases included at category (b) and category
266 (c).

267 2.5 Decision-Making Model (AHP technique)

268 The AHP technique is commonly employed in decision-making systems designed to aid in decision-making and rate options
269 (Saaty, 1986). Actual metrics such as pricing, headcount, or subjective opinions are used as inputs into a numerical matrix in
270 AHP. Ratio scales and consistency indices derived from eigenvalues and eigenvectors are among the results. The AHP model
271 is a decision-making framework that assumes decision levels have a unidirectional hierarchical relationship (Presley, 2006).
272 AHP can study the interrelationships among all criteria using the hierarchical approach (Singh et al., 2007).

273 According to (Albayrak and Erensal, 2004), there are three processes that go into creating AHP: model structure
274 (decomposition), comparative judgment of alternatives and criteria, and priority synthesis. These methods can be broken down
275 into four stages.

276 In the first stage, AHP divides a complex multi-criteria decision problem into a hierarchy of interrelated elements (criteria,
277 decision alternatives). The criteria and alternatives are arranged in a family tree-like hierarchical structure. The next stage,
278 after the problem has been decomposed and a hierarchy has been established, is to begin the comparison judgment process to
279 evaluate the relative importance of the criteria within the grade. The criteria are compared pairwise at each grade based on
280 their degrees of influence and the criteria provided at the higher grade. Pairwise comparisons are based on a nine-point scale,
281 with 1 indicating "equal importance," 3 indicating "slightly more important," 5 indicating "much more important," 7 indicating
282 "highly more important," and 9 indicating "extremely more important" (Issa et al., 2020; Abdelwahab et al., 2021). These
283 alternatives and criteria are evaluated based on the subjective opinions of experts represented by a point scale, including any
284 intermediate value (2, 4, 6, and 8).

285 As demonstrated in Eq. (5), the result of a pairwise comparison on n criteria can be summarized in a $[X]_{(n \times n)}$ evaluation matrix.

$$\begin{array}{l}
 288 \\
 289 \\
 290 \\
 291 \\
 292
 \end{array}
 \begin{array}{l}
 C_1 \quad C_2 \quad \dots \quad C_n \\
 \left[\begin{array}{cccc}
 x_{11} & x_{12} & \dots & x_{1n} \\
 x_{21} & x_{22} & \dots & x_{2n} \\
 \vdots & \vdots & \ddots & \vdots \\
 x_{n1} & x_{n2} & \dots & x_{nn}
 \end{array} \right] \begin{array}{l}
 C_1 \\
 C_2 \\
 \\
 C_n
 \end{array}
 \end{array}
 \quad (5)$$

293 Where: $c_j = 1, 2, 3 \dots n$ – the set of criteria; x_{ij} ($ij = 1, 2, 3 \dots n$) – the weight quotient of the criteria; $x_{ij}=1$; $x_{ji}=1/x_{ij}$; $x_{ij} \neq 0$

294 The third stage, which comes after the dual comparison matrices, is to calculate the eigenvector, which shows the importance
 295 of each element in the relevant matrix with respect to the others (Albayrak and Erensal, 2004).

296 In Eqs (6) and (7), the % importance distribution of criterion is computed as follows:

$$297 \quad b_{ij} = \frac{x_{ij}}{\sum_{i=1}^n x_{ij}} \quad (6)$$

$$298 \quad w_i = \frac{\sum_{j=1}^n b_{ij}}{n} \quad (7)$$

299 Where: b_{ij} – the values of the normalized matrices; $[w_i]_{n \times 1}$ – the percentage importance distribution of criteria; n – the
 300 number of criteria.

301 The fourth step is to ensure that the consistency ratio (CR) for each comparison matrix does not exceed 10% at the most.

302 A CR greater than 10% indicates inconsistency in the decision maker's judgments. The judgments in this case should be
 303 improved. Eqs (8) and (9) are used to compute the CR value:

$$304 \quad [D_i]_{n \times 1} = [x_{ij}]_{n \times n} * [w_i]_{n \times 1} \quad (8)$$

$$305 \quad \lambda_{max} = \frac{\sum_{i=1}^n \frac{d_i}{w_i}}{n} \quad (9)$$

306 Where: λ_{max} is the matrix's largest eigenvector and $[D_i]_{n \times 1}$ is the weighted matrix.

307 Random Index (RI) is another value required to calculate CR. (Özat, 2013) provides the data, which includes the RI values, which
 308 are constant numbers determined by the N value. Eq. (10) specifies the calculation of the CR value based on this information.

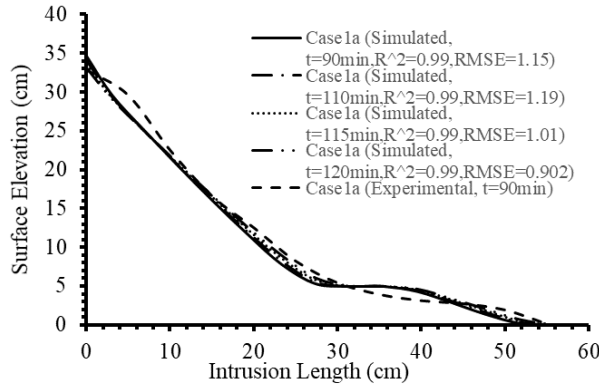
$$309 \quad CR = \frac{\lambda_{max} - n}{(n-1) * RI} \quad (10)$$

310 Where CR is the consistency ratio, λ_{max} is the matrix's largest eigenvector, RI is the random index, and n is the number of criteria.

311 In this study, it is suggested that an AHP-based model be used on two levels to find the best model case by comparing these
 312 model cases with the help of many ratios as a selection criterion. Through the AHP analysis, the model cases will be named as
 313 alternatives. The three alternatives (cases 1a, 1b, and 1c) with no vertical barrier countermeasure will be eliminated from the
 314 total number of alternatives, 21 alternatives, reducing the total number of alternatives to 18 alternatives (six cases in each
 315 category). Level (1) involves the model dealing with three categories (a, b, and c) in order to select the best alternative from
 316 each. There are four criteria in category (a) (Rr, SLR_i, Minimum HHR, and WAR), and five in categories (b) and (c), with
 317 RER which is indicating the artificial recharge, which is exclusively utilized in categories (b) and (c). The top three alternatives
 318 from each of the three categories that emerged from level (1) can be used to create the final choice for the best alternative at
 319 level (2). Pairwise comparisons with other criteria aid in determining the relative importance of each criterion in the
 320 hierarchical structuring of the problem. The model's first level consists of one matrix (4x4) for category (a) alternatives and
 321 one matrix (5x5) for categories (b) and (c) alternatives, reflecting the relative weights of the criteria as outputs. Moreover, five
 322 matrices (6x6) show the relative weight among the alternatives in the case of each criterion. The model, on the other hand,
 323 takes the same matrix for criteria weights and five matrices, each of which is (3x3), and expresses the relative weight among
 324 the final three alternatives for each criterion in its second level.

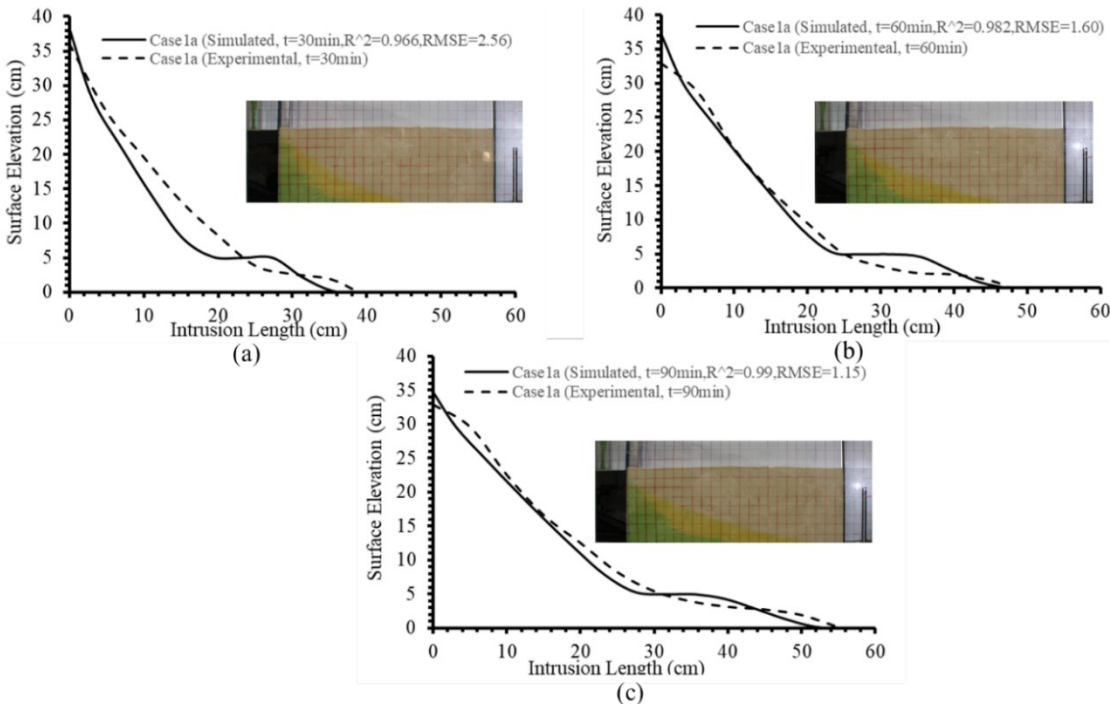
326 3.1 Calibration and Verification of the Numerical Model

327 The steady-state condition in experiment 1 (the base case) occurs 90 minutes after the experiment begins. As a validation of
 328 the numerical model steady-state simulation, **Figure 8** shows the observed and simulated saltwater lines for various simulation
 329 times greater than 90 minutes. The figure shows that the simulated saltwater line closely matches the observed one, with RMSE
 330 values ranging from 0.90 to 1.19 for time ranging from 90 to 120 minutes which confirm the occurrence of a steady-state
 331 condition after 90 minutes.

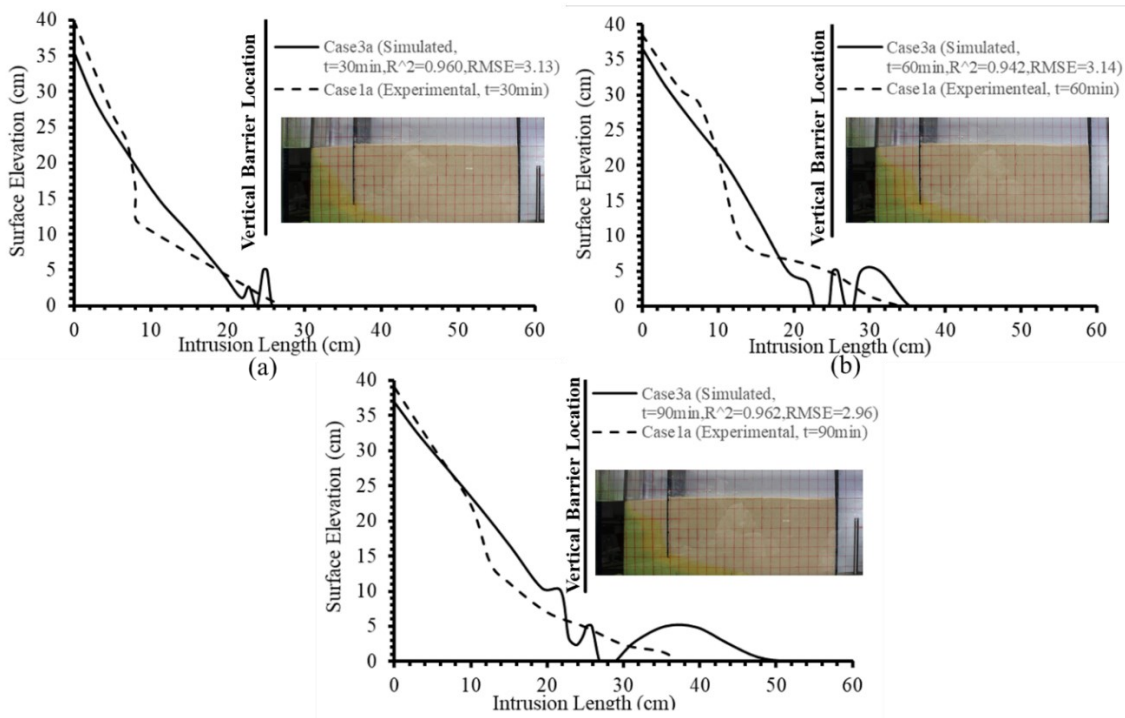


332 **Figure 8: Observed and simulated saltwater lines for experiment 1 (Case1a) under steady-state conditions at intervals longer than**
 333 **90 minutes.**

334 For transient results, the saltwater line for experiments 1 and 2 for simulation times of 30, 60, and 90 minutes is used to verify
 335 the corresponding results of the numerical model, as shown in **Figure 9** and **Figure 10**. Both figures show that the model
 336 produces reasonable simulated results for the saltwater lines (case3a) when compared to the observed ones. **Table 5** also
 337 shows the calibrated hydrogeological properties of the verified numerical model, including hydraulic conductivities in X, Y,
 338 and Z directions (k_x, k_y, k_z), specific yield (S_y), specific storage (S_s), and effective porosity (η). The upcoming analysis will
 339 consider the results at 90 minutes as a steady-state condition.
 340



341 **Figure 9: Observed and simulated saltwater lines for experiment1 (Case1a) for transient state condition: (a) 30min, (b) 60min, (c)**
 342 **90min**



344
 345 **Figure 10: Observed and simulated saltwater lines for experiment2 (Case3a) for transient state condition: (a) 30min, (b) 60min, (c)**
 346 **90min**

347 **Table 5: Calibrated values of the hydrogeological properties**

Hydrogeological Properties	$k_x(cm/s)$	$k_y(cm/s)$	$k_z(cm/s)$	S_y	S_s	η
Values	0.0069	0.0069	0.03	0.04	0.0619	0.0428

348

349 3.2 Behavior evaluation of saltwater intrusion, flow, and hydraulic heads for categories (a), (b), and (c) model cases

350 3.2.1 Saltwater intrusion and flow behaviors in category(a) model cases

351 The modeling results of saltwater intrusion and the accompanying flow behavior for the cases in category (a) will be discussed
 352 in this section. Two evaluation ratios are considered, including IR and the SLR_{avg} . Moreover, conditional parameters (BDR)
 353 and geometrical parameters (LR and DR) will be considered through the discussion. **Figure 11** depicts these outcomes, and
 354 **Table 6** provides a summary of the results.

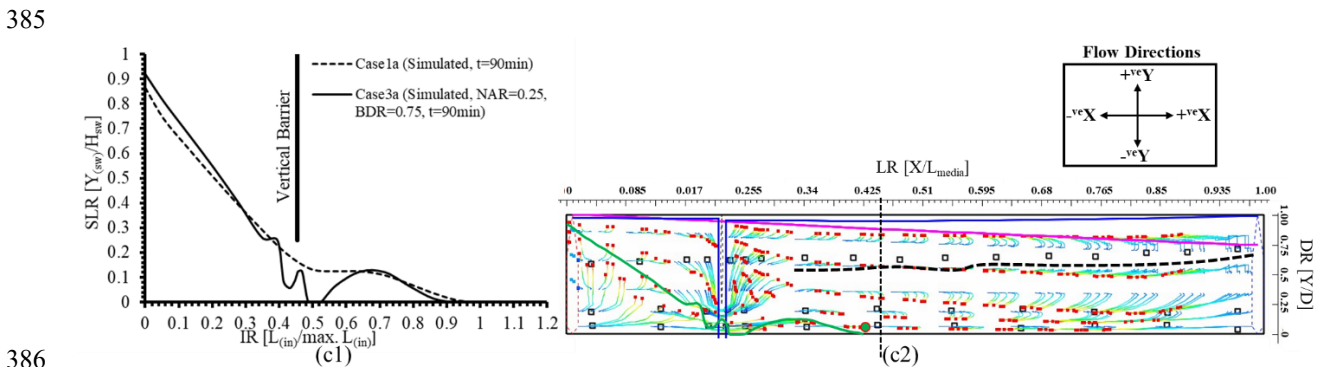
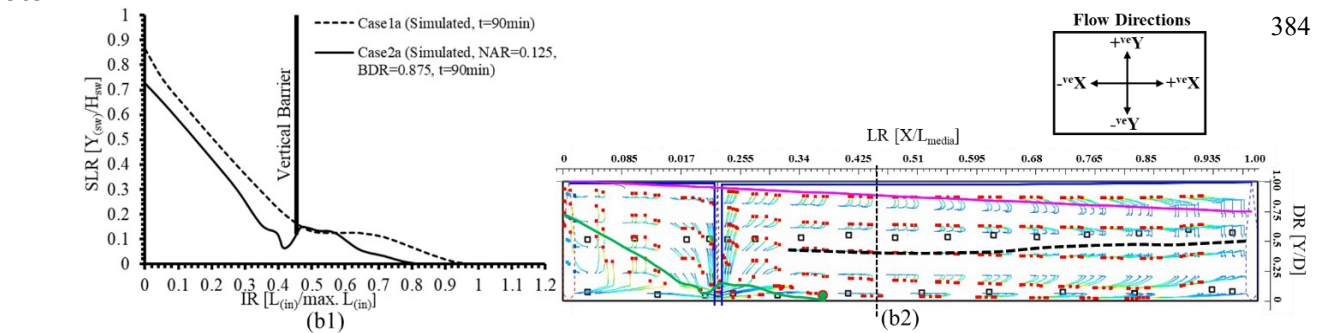
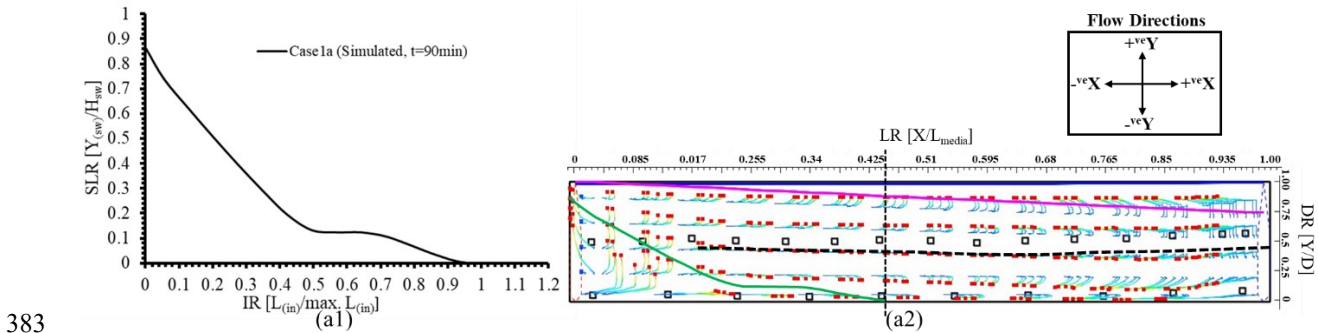
355 Figures from **Figure 11a1** to **Figure 11g1** as well as

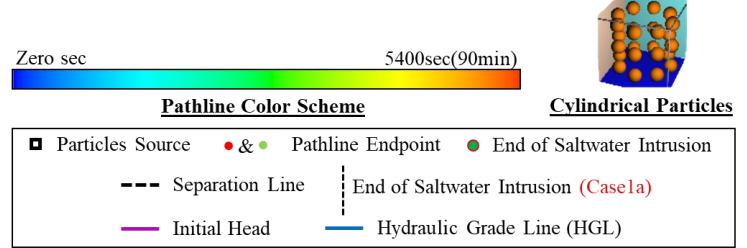
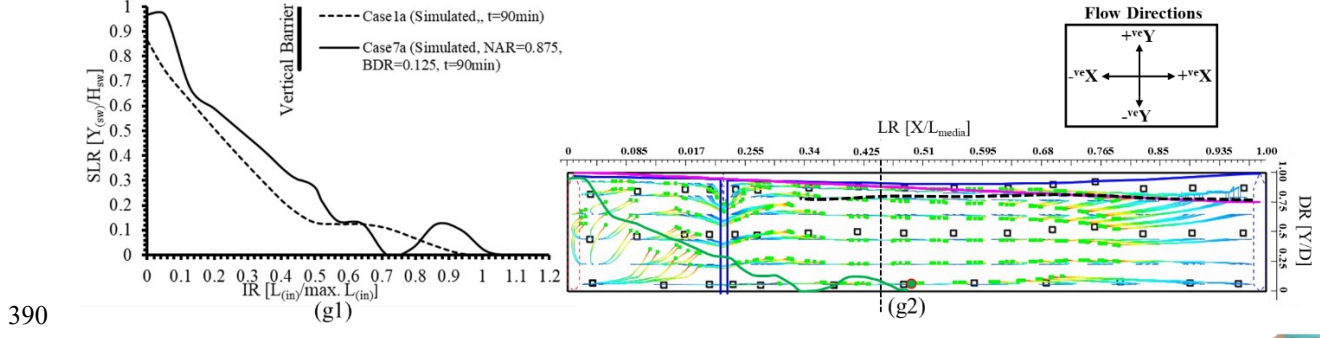
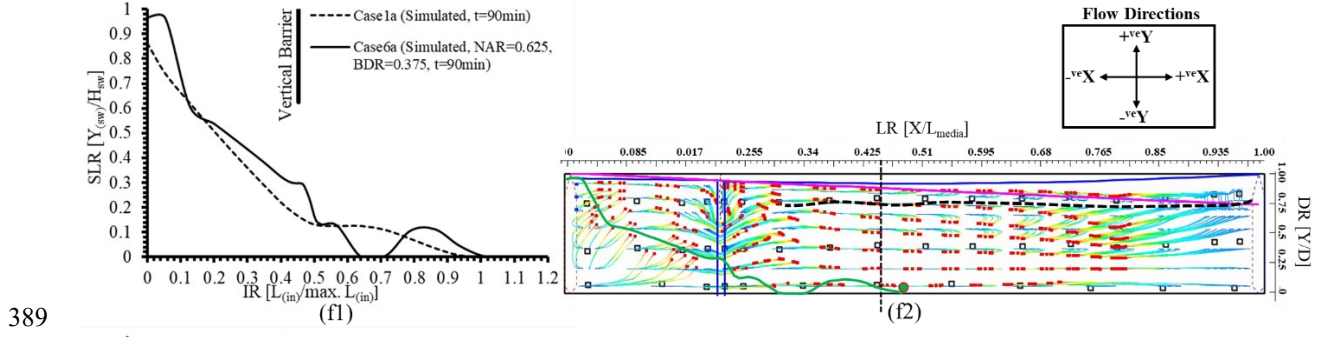
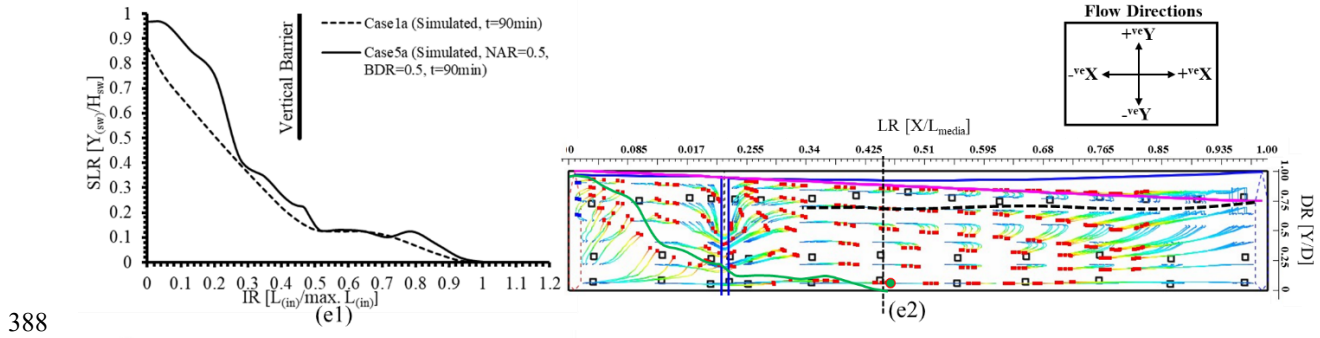
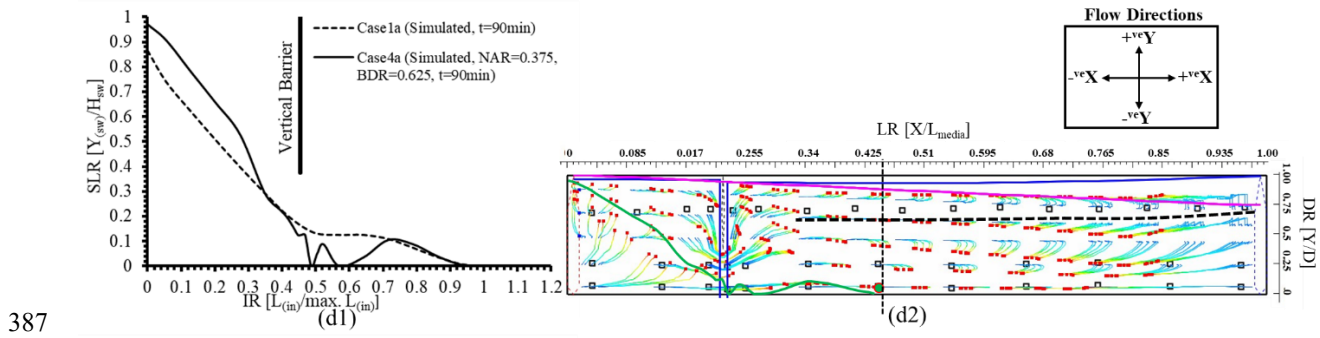
356 **Table 6** reveal that case 2a, which uses a vertical barrier with high BDR values, has the lowest evaluation ratio values (see
 357 **Figure 11b1**). Case 7a's evaluation ratios, on the other hand, have the highest values when a vertical barrier with low BDR
 358 values is applied (see **Figure 11g1**). Given these findings, flow behavior through the media sand needs to be investigated as
 359 an explanation for the variation in evaluation ratios.

360 Figures from **Figure 11a2** to **Figure 11g2** depict the flow behavior of freshwater and saltwater. **Figure 11a2** depicts the flow
 361 behavior of case1a, demonstrating that the flow in zone1 takes two directional flows: $+^{ve}Y$ and $+^{ve}X$. The $+^{ve}Y$ flow conserves
 362 hydraulic heads near the saltwater boundary at the media sand level. Furthermore, the $+^{ve}X$ flow forces freshwater above the
 363 saltwater line to flow in the same direction as the saltwater. Freshwater flow directions in zone 2 are $-^{ve}X$ and $+^{ve}Y$ in the upper
 364 half of the zone and $-^{ve}X$ and $-^{ve}Y$ in the lower half of the zone. Because of the $+^{ve}Y$ and $-^{ve}Y$ flows in zone 2, a separation line
 365 with a DR value in the range of 0.37 to 0.45 could be identified, as illustrated in

366 **Table 6** and shown in **Figure 11a2**. Along zone2, the $+^{ve}Y$ flow direction conserves hydraulic head. In the upcoming analysis,
 367 the DR value of the separation line will be termed $DR_{separation}$.

368 **Figure 11b2** shows that the vertical barrier impedes freshwater flows from zone2a to zone2b, creating overlaying pressure in
 369 zone1a, resulting in a dramatic drop and rise of the saltwater line shortly before and after the vertical barrier. Moreover, as
 370 shown in
 371 **Table 6**, the value of $DR_{\text{separation}}$ increases to be in the range of 0.40 to 0.50 when compared to case1a.
 372 The flow of freshwater from zone2a to zone2b is boosted by continuing to decrease BDR values, producing fluctuations in the
 373 saltwater line. Because of this flow, the overlying pressure of freshwater on zone 1a is reduced, leading the SLR value in this
 374 zone to rise (see **Figures 11c2, 11d2, 11e2, 11f2, 11g2**). Furthermore, these figures and
 375 **Table 6** show that $DR_{\text{separation}}$ values are increasing, indicating that the majority of the freshwater flow in zone 2b is in the -veY
 376 flow direction, resulting in hydraulic head reduction through this zone.
 377 Based on the given results, it is possible to conclude that case2a has the lowest evaluation ratio values among the other cases.
 378 Furthermore, large $DR_{\text{separation}}$ values, such as case7a, limit the hydraulic heads, creating an excess increase in the evaluation
 379 ratios (see **Figure 11g1 and Figure 11g2**). In addition, adopting a vertical barrier with a high BDR ratio could effectively
 380 manage the saltwater intrusion. Furthermore, management of saltwater intrusion will be considered in this study by managing
 381 the $DR_{\text{separation}}$ as well as the hydraulic heads along zone2b using groundwater artificial recharge in conjunction with the use of
 382 a vertical barrier.





391
 392 **Figure 11: Simulated saltwater lines and groundwater flow behavior of the category (a) model cases: (a) case1a, (b) case2a, (c) case**
 393 **3a, (d) case4a, (e) case5a, (f) case6a, (g) case7a**

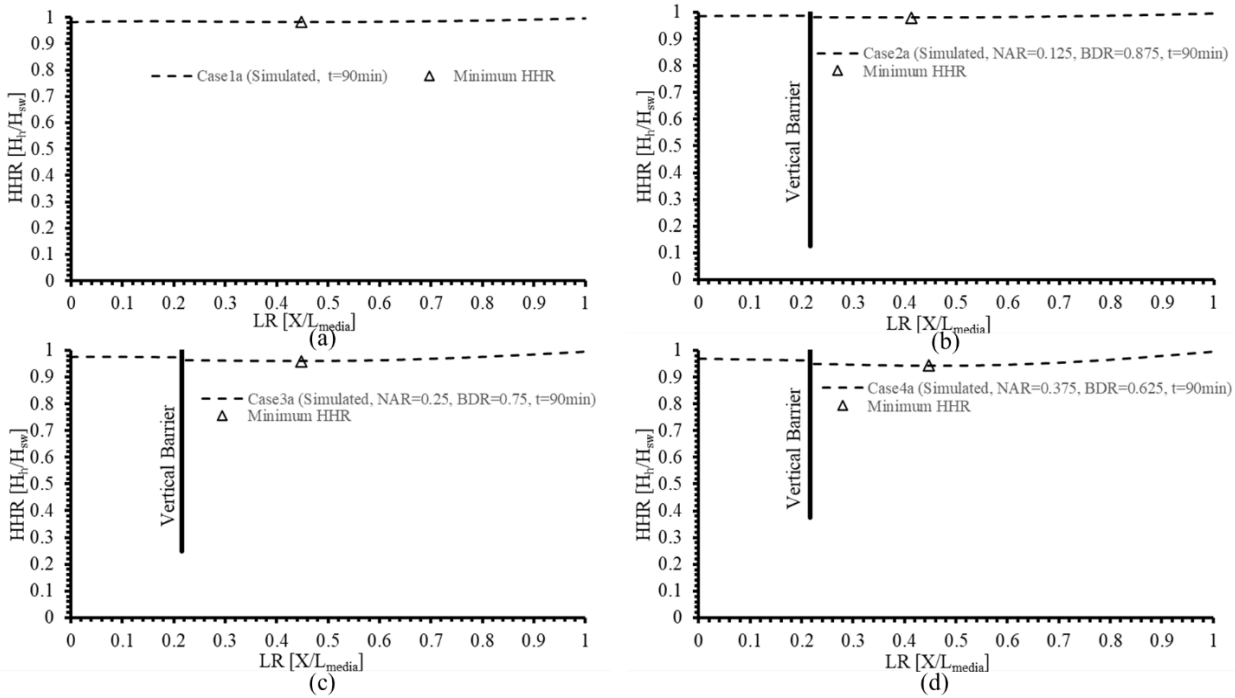
394
 395
 396
 397
 398
 399
 400

401 **Table 6: Values of the evaluation ratios and DR values for category (a) model cases**

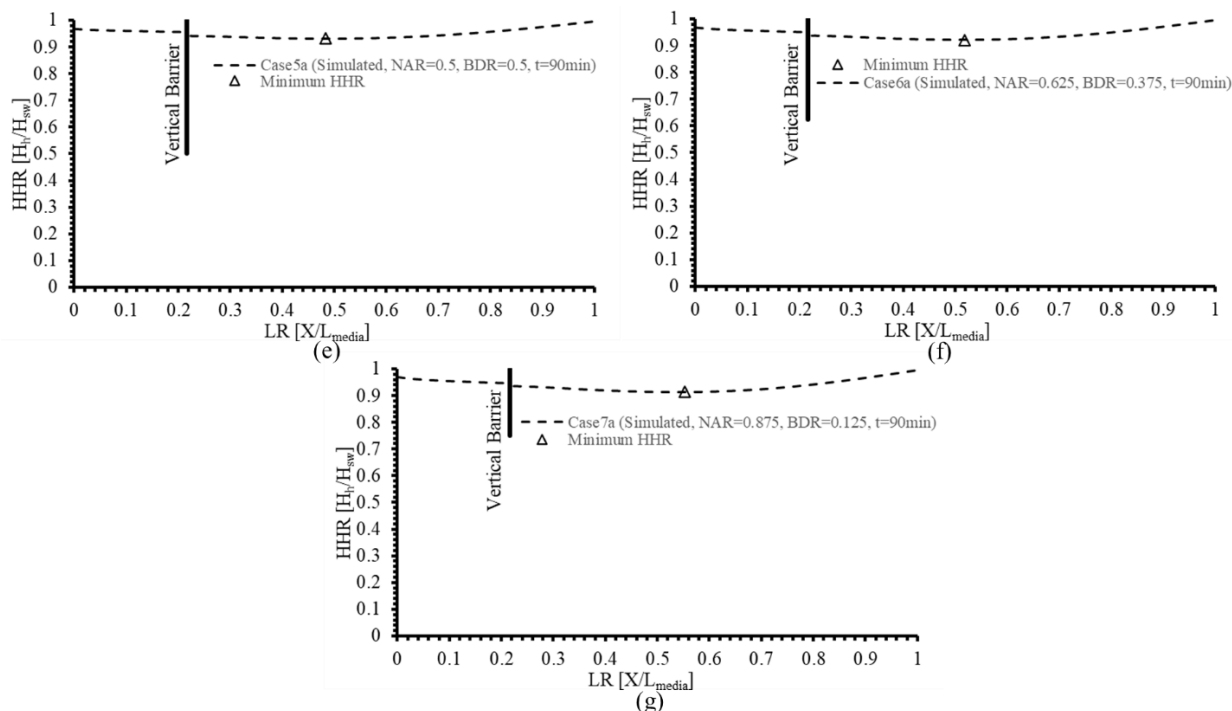
Cases	Conditional Parameters	Evaluation Ratios		Geometrical Parameters	
	BDR	IR	SLR _{avg}	LR _{Intrusion}	DR _{separation}
Case1a	---	0.97	0.28	0.45	0.37-0.45
Case2a	0.875	0.83	0.20	0.39	0.40-0.50
Case3a	0.75	0.90	0.23	0.42	0.50-0.68
Case4a	0.625	0.97	0.25	0.45	0.60-0.70
Case5a	0.50	0.97	0.31	0.45	0.69-0.75
Case6a	0.375	1.05	0.29	0.48	0.71-0.78
Case7a	0.125	1.05	0.32	0.48	0.76-0.85

402 **3.2.2 Hydraulic head variations in category(a) model cases**

403 As illustrated in **Figure 12**, the hydraulic head variations indicated by the HHR evaluation ratio are investigated for the
 404 category(a) model cases. This figure illustrates the relationship between HHR and LR ratios by displaying the minimum HHR
 405 values and their locations along the aquifer. **Figure 12** shows that the hydraulic head of case7a has the lowest HHR value of
 406 0.91 compared with the other cases (cases 1a-6a) located at a LR value of 0.55 (see **Figure 12g**). On the other hand, Casela,
 407 has the highest value of the minimum HHR (0.98), and a location has a LR of 0.44, as shown in **Figure 12a**.

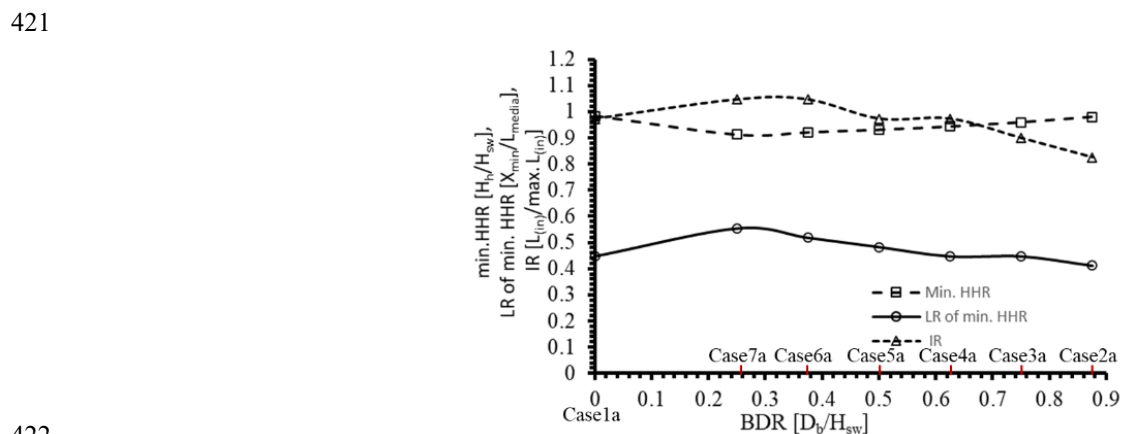


408



409
410 **Figure 12: Values and locations of the minimum HHR of the category (a) model cases: (a) case1a, (b) case2a, (c) case 3a, (d) case4a,**
411 **(e) case5a, (f) case6a, (g) case7a**

412 The above results can be summarized as illustrated in **Figure 13**, which depicts the effect of BDR on the location (LR), the
413 value of the minimum HHR, and the IR ratios. The minimum hydraulic head is located at zone2b for all study cases (case1a-
414 case7a), with LR values ranging from 0.45 to 0.55 and corresponding minimum HHR values ranging from 0.91 to 0.98. On
415 the other hand, the maximum IR occurs for both cases 6a and 7a with a value of 1.05 when using a BDR in the value range
416 from 0.25 to 0.38. Given these findings, increasing the hydraulic head represented by HHR could effectively control saltwater
417 intrusion when combined with the vertical barrier countermeasure. For this purpose, using groundwater artificial recharge,
418 whether by surface or subsurface recharge, at the location of the minimum HHR value (LR in the range from 0.45 to 0.55),
419 combined with the use of a vertical barrier, could be used to control saltwater intrusion, as will be discussed in the following
420 sections of this study.



422
423 **Figure 13: Effect of BDR on the IR and minimum HHR values and locations**

424 3.2.3 Saltwater intrusion and flow behaviors in categories (b) and (c) model cases

425 Groundwater artificial recharge is used to control saltwater intrusion in zone2b along the LR range (from 0.45 to 0.55), which
426 has a minimum value of HHR for preserving its value at the unity value. Surface and subsurface recharge are numerically
427 discussed, either separately or in conjunction with the vertical barrier, as shown in Error! Reference source not found. for
428 category (b) and category (c) model cases. The recharge is applied along the whole range of LR values from 0.45 to 0.55 for
429 surface recharge. In contrast, for subsurface recharge, the recharge is applied as a line of wells at the midpoint of the same LR

430 range at a value of 0.5. The results of category (b) and category (c) study cases will be compared with the base case results
 431 (case1a) and the corresponding cases of category (a) in the following discussions, as depicted in **Figure 14** and summarized
 432 in **Table 8**.

433 As an analysis of the saltwater intrusion based on the evaluation ratios from **Figure 14a1** to **Figure 14g1** as well as **Table 8**,
 434 it is found that case3b has the lowest IR value among all the model cases included in categories (a), (b), and (c). However, the
 435 SLR_{avg} values of case2a and case3b are the lowest, with case2a having a lower value than case3b.

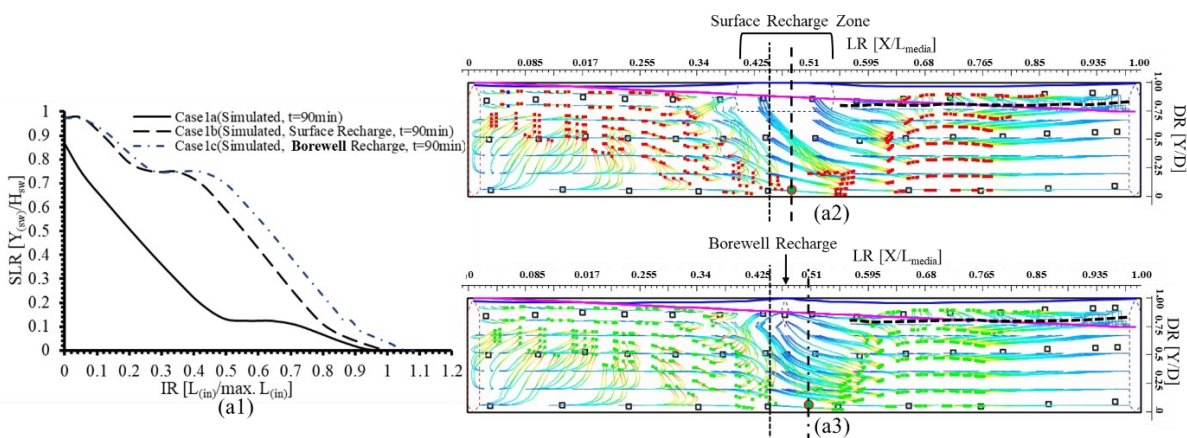
436 The saltwater and freshwater flow behaviors could be described from **Figure 14a2** to **Figure 14g2**. In case1b, the surface
 437 recharge works as a hydraulic barrier that prevents saltwater from flowing in the ^{+ve}X direction as well as forces it to flow
 438 intensively in the ^{+ve}Y direction. This behavior causes an increase in the SLR_{avg} , compared with that of case1a, and the majority
 439 of recharged freshwater is forced to take a ^{+ve}X direction (see **Figure 14a2**). The flow behavior in case1c is similar to that in
 440 case1b (see **Figure 14a3**), but its SLR_{avg} is higher, indicating that the countermeasure effect of subsurface recharging, which
 441 is a line of wells, is less than that of surface recharge, which is a water mass.

442 In contrast to Case 2b, the value of SLR rises due to the ^{-ve}X flow direction of surface recharge towards the neck area beneath
 443 the vertical barrier, preventing the saltwater line from intruding (**Figure 14b2**). Because well recharge has a lower effect than
 444 surface recharge, the IR and LR ratios are higher in case 2c than in case 2b, as shown in **Figures 14b2** and **14b3** and illustrated
 445 in **Table 8**.

446 In the case3b flow behavior, freshwater flows intensively from zone 2a to zone 2b (see **Figure 14c2**), causing SLR_{avg} to decline
 447 to become the least among the category (b) model cases. Because of the poor influence of well recharge, the SLR_{avg} value for
 448 case3c is greater than that of case3b, as demonstrated in **Table 8**. By continuing to lower BDR for cases 4b, 5b, 6b, and 7b, as
 449 well as the corresponding cases in category (c), the freshwater flows from zone 2a to zone 2b in the ^{+ve}X direction, which
 450 reduces the effect of surface and well recharge, as shown in **Table 8**.

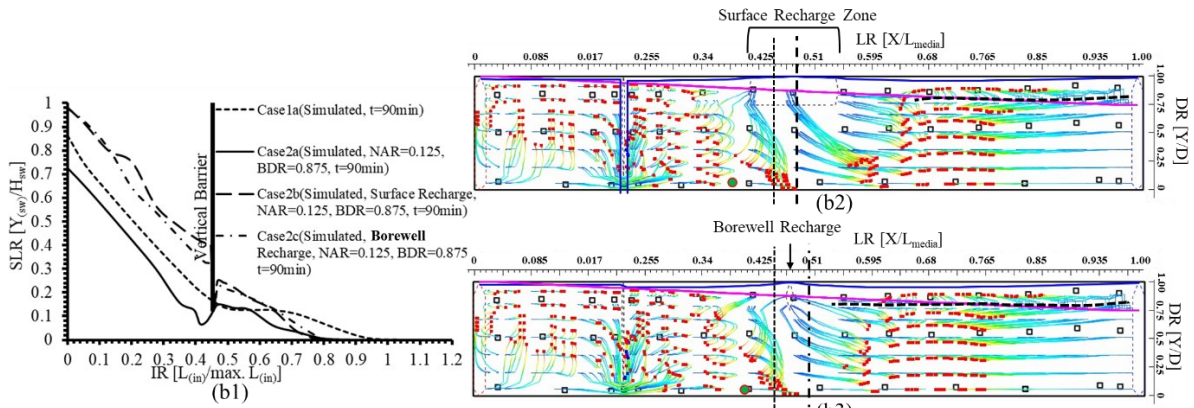
451 Because of the artificial recharge that applies in categories (b) and (c), the hydraulic heads along the experiment section are
 452 unchanged for all model cases, and the $DR_{separation}$ is nearly the same with a value range from 0.75 to 0.90.

453 Based on the findings, it is possible to conclude that artificial aquifer recharging along the LR values from 0.45 to 0.55, which
 454 has a minimum value of the HHR ratio to conserve its value, as well as the unity accompanied by using a vertical barrier, has
 455 a significant effect on controlling saltwater intrusion. Furthermore, because of its body mass, surface recharge is more efficient
 456 than well recharge. Conclusively, the value of IR, as an evaluation ratio, for case3b is the lowest among the whole cases
 457 included in categories (a), (b), and (c). However, the minimum value of SLR_{avg} is achieved in case2a, confirming the efficient
 458 combination of the vertical barrier and surface recharge at the location of the minimum HHR (LR in the range from 0.45 to
 459 0.55).

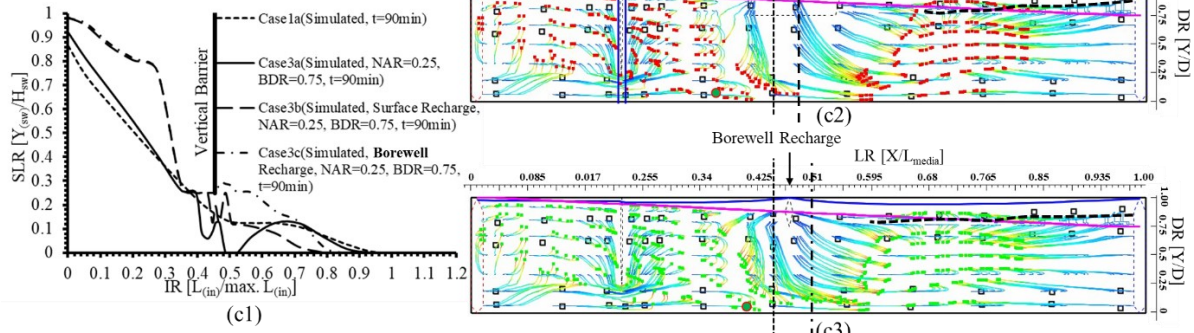


460

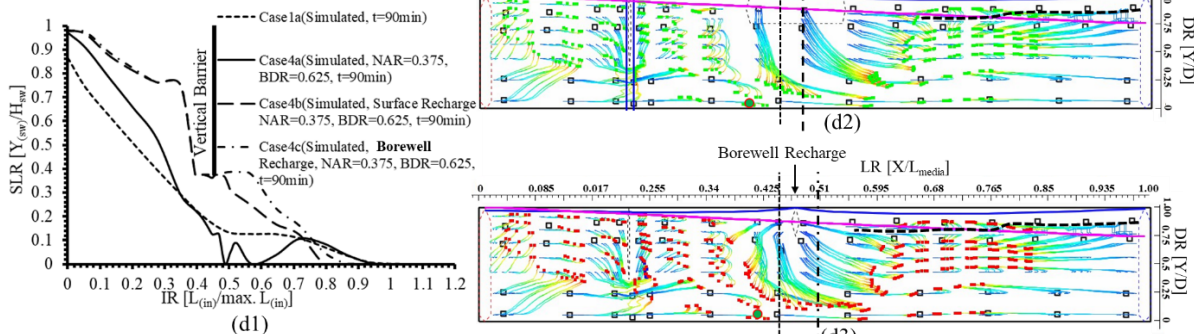
461



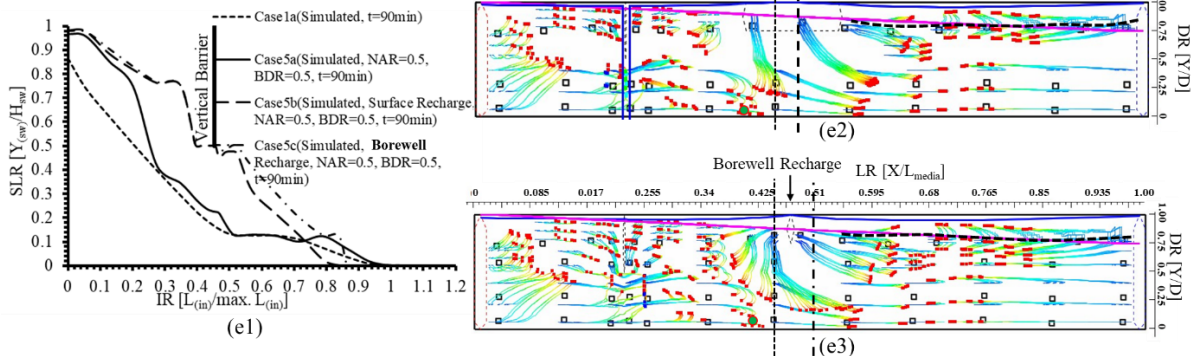
462



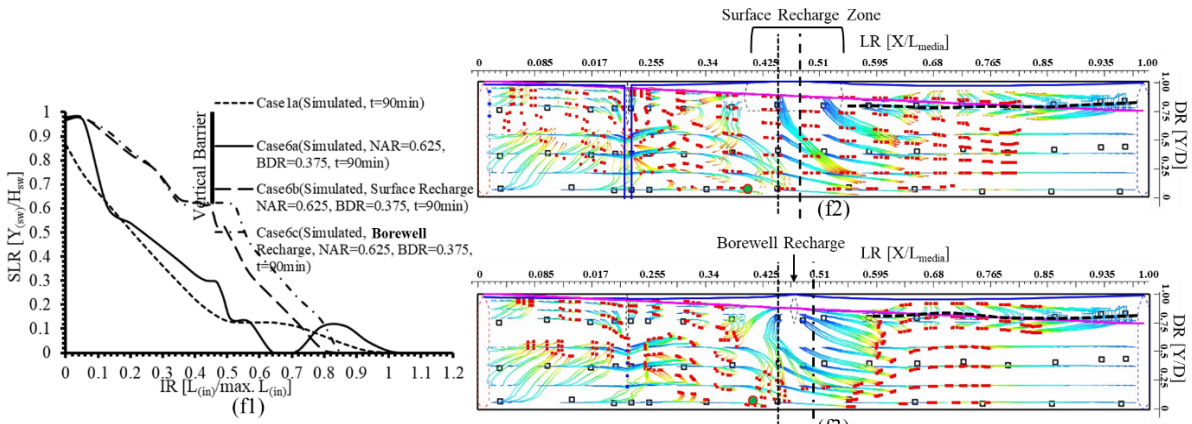
463



464

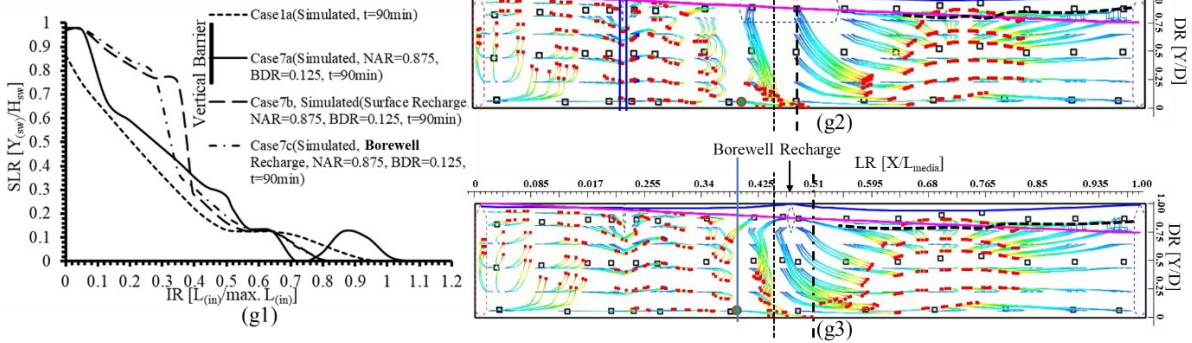


465

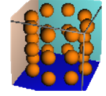


466

467

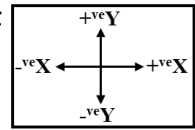


Zero sec 5400sec(90min)

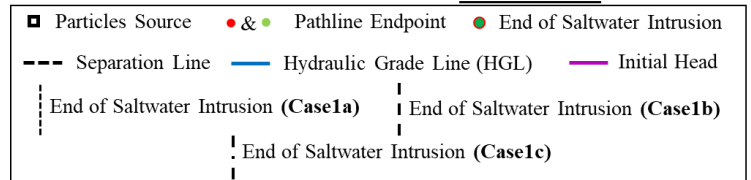


Cylindrical Particles

Pathline Color Scheme



Flow Directions



468

469

470

Figure 14: Simulated saltwater lines and groundwater flow behavior of the category (b) and (c) model cases: (a) case1b &1c, (b) case2b&2c, (c) case 3b&3c, (d) case4b&4c, (e) case5b&5c, (f) case6b&6c, (g) case7b&7c

471

472

473

474

475

476

477

478

479

480

481

482

483

484

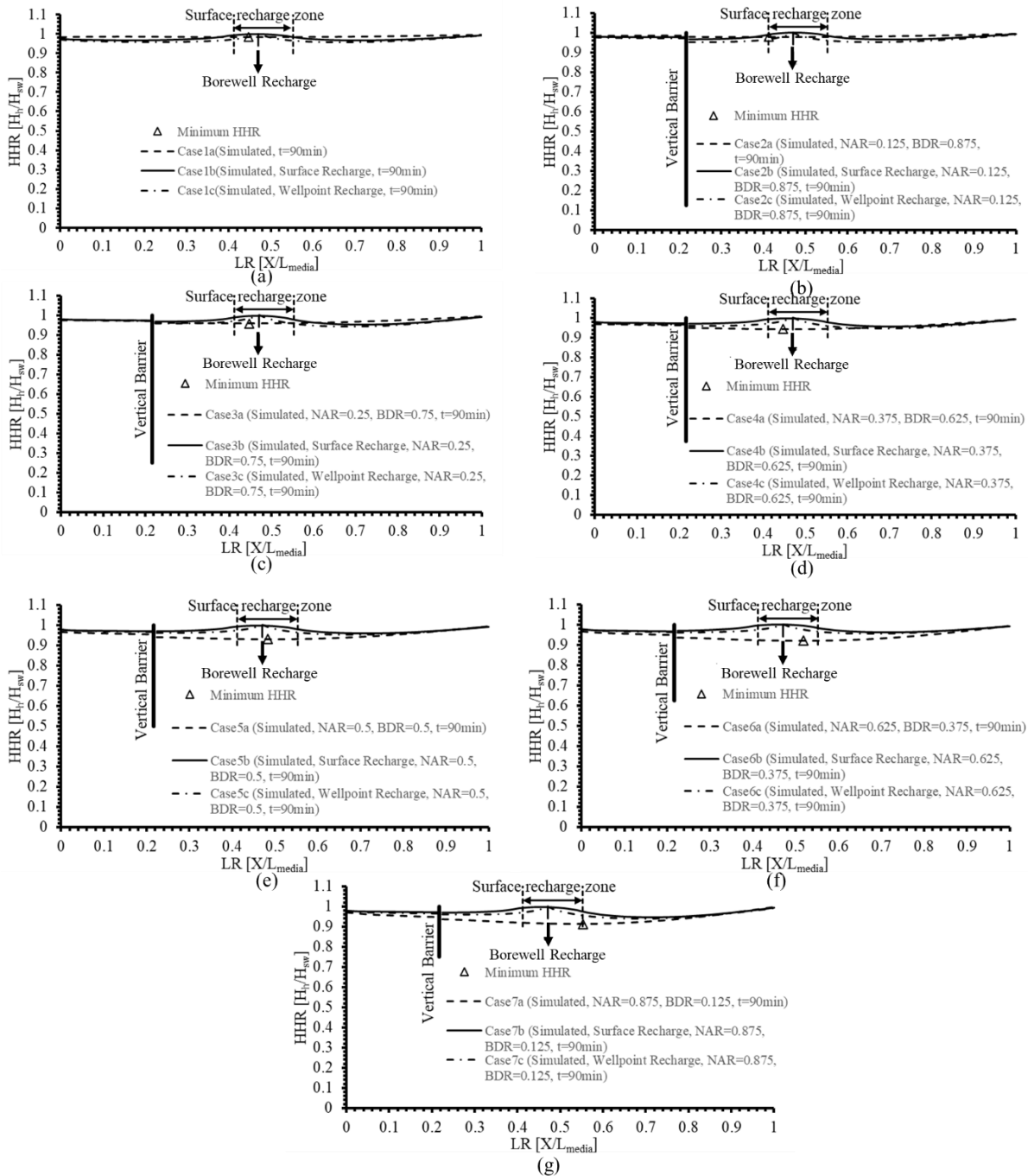
485

486 **Table 7: Values of the evaluation ratios and DR values for category (a) model cases**

Category	Cases	Conditional Parameters	Evaluation Ratios		Geometrical Parameters	
		BDR	IR	SLR _{avg}	LR _{Intrusion}	DR _{separation}
Category(a)	Case1a	---	0.97	0.28	0.45	0.37-0.45
	<u>Case2a</u>	<u>0.875</u>	<u>0.83</u>	<u>0.20</u>	<u>0.39</u>	<u>0.40-0.50</u>
	Case3a	0.75	0.90	0.23	0.42	0.50-0.68
	Case4a	0.625	0.97	0.25	0.45	0.60-0.70
	Case5a	0.50	0.97	0.31	0.45	0.69-0.75
	Case6a	0.375	1.05	0.29	0.48	0.71-0.78
	Case7a	0.125	1.05	0.32	0.48	0.76-0.85
Category(b)	Case1b	---	1.0	0.39	0.47	0.80-0.85
	Case2b	0.875	0.75	0.40	0.35	0.80-0.85
	<u>Case3b</u>	<u>0.75</u>	<u>0.68</u>	<u>0.34</u>	<u>0.32</u>	<u>0.80-0.90</u>
	Case4b	0.625	0.81	0.44	0.38	0.80-0.90
	Case5b	0.50	0.81	0.51	0.38	0.75-0.80
	Case6b	0.375	0.81	0.54	0.38	0.75-0.80
	Case7b	0.125	0.81	0.37	0.38	0.80-0.90
Category(c)	Case1c	---	1.05	0.41	0.49	0.80-0.85
	Case2c	0.875	0.82	0.35	0.38	0.80-0.85
	Case3c	0.75	0.82	0.38	0.38	0.80-0.90
	Case4c	0.625	0.85	0.45	0.40	0.80-0.90
	Case5c	0.50	0.85	0.52	0.40	0.75-0.80
	Case6c	0.375	0.85	0.57	0.40	0.75-0.80
	Case7c	0.125	0.75	0.39	0.40	0.80-0.90

487 **3.2.4 Hydraulic head variations in categories (b) and (c) model cases**

488 **Figure from 15a to 15g** depict the hydraulic heads along the aquifer as represented by the HHR ratio for cases in categories
489 (b) and (c) compared to category (a). The hydraulic heads for all cases have been conserved along the LR ratio from 0.45 to
490 0.55, which has the minimum value of HHR to have the unity value, and the losses through the vertical barrier are greatly
491 reduced when compared to those of category (a).



492

493

494 **Figure 15: Hydraulic head variation along the aquifer for categories (b) and (c) compared with those of category (a) model cases:**
 495 **(a) case1a&1b&1c, (b) case2b&2b&2c, (c) case 3b&3b&3c, (d) case4b&4b&4c, (e) case5b&5b&5c, (f) case6b&6b&6c, (g)**
 496 **case7b&7b&7c**

497 **3.3 Classification of model cases**

498 The classification ratios described in Section 2.3.2, Classification Ratios, are summarized and classified in **Figure 16** and
 499 **Table 8**. **Figure 16a** presents the SLR_{avg} and R_r values for each model case, whereas **Figure 16b** depicts the WAR and RER
 500 values. **Figures 16** and **Table 8** show that case3b has the best R_r value of 0.29. Case2a, on the other hand, has the best SLR_{avg}
 501 and WAR values of -0.08 and 0.76, respectively. Furthermore, case7c has the best RER value of 1.91. On the contrary, case1c
 502 has the worst R_r and WAR values of -0.07 and 2.18, respectively. Furthermore, case6b has the worst RER value of 3.62.
 503 Moreover, case6c has the worst SLR_{avg} value of 3.62. The remaining model cases are categorized as unclassified model cases.
 504 Based on the findings, it is difficult to determine which model case is the most successful scenario to implement as a saltwater
 505 intrusion countermeasure. As a result, the DMM model is needed for determining the most effective model case.

506

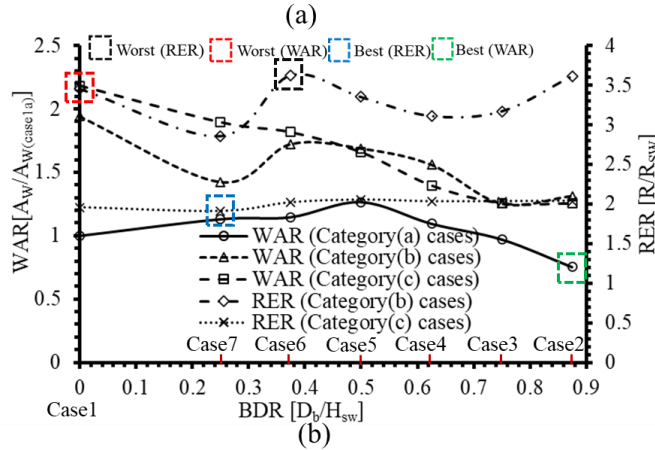
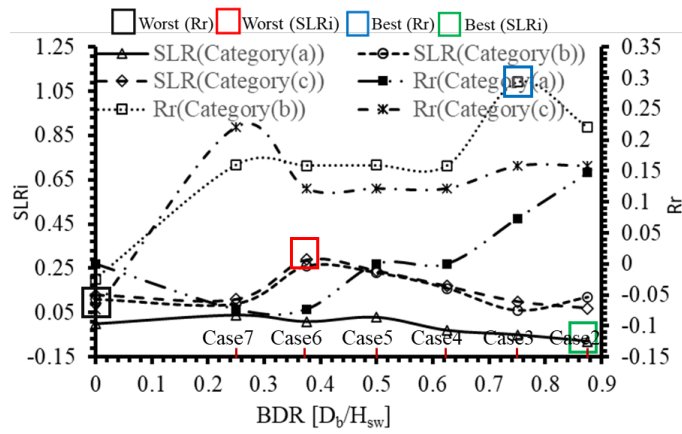


Figure 16: Classifications of model cases included in categories (a), (b), and (c): (a) SLR_{avg} and R_r values, (b) WAR and RER values

Table 8: Model cases classification according to values of classification ratios

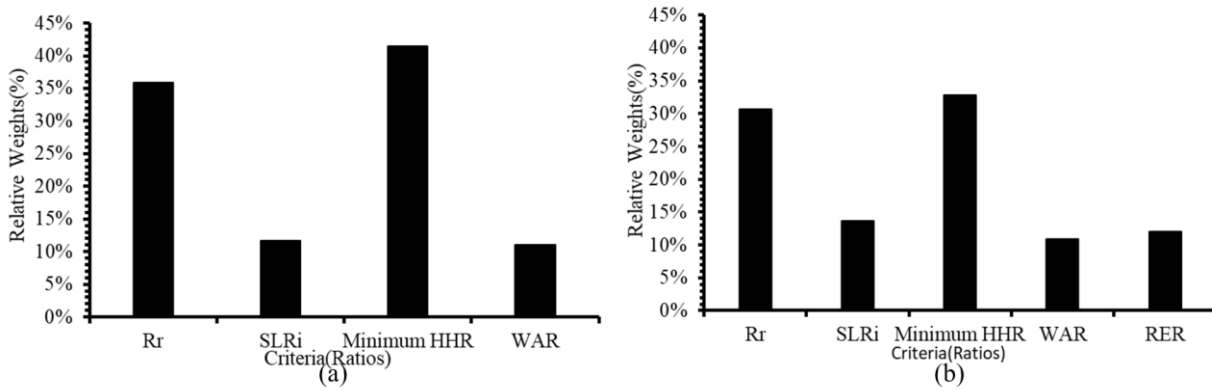
Classification Ratio	Best	Worst
SLR_i	Case2a (-0.08)	Case6c (0.29)
R_r	Case3b (0.29)	Case1c (-0.07)
WAR	Case2a (0.76)	Case1c (2.18)
RER	Case7c (1.91)	Case6b (3.62)

3.4 Selecting the Most Effective Model Case (AHP application results)

As previously stated, the AHP model is applied to the numerical model results at two different levels of selection (levels (1) and (2)). Model cases are referred to as alternatives at this stage, and selected ratios among the evaluation and classification ratios are referred to as criteria. Level (1) needs to determine the best alternative in each category. Furthermore, level (2) is for deciding the best alternative. For category (a) alternatives, the criteria values used include SLR_i , minimum HHR, R_r , and WAR, and the RER is added over these ratios for categories (b) and (c).

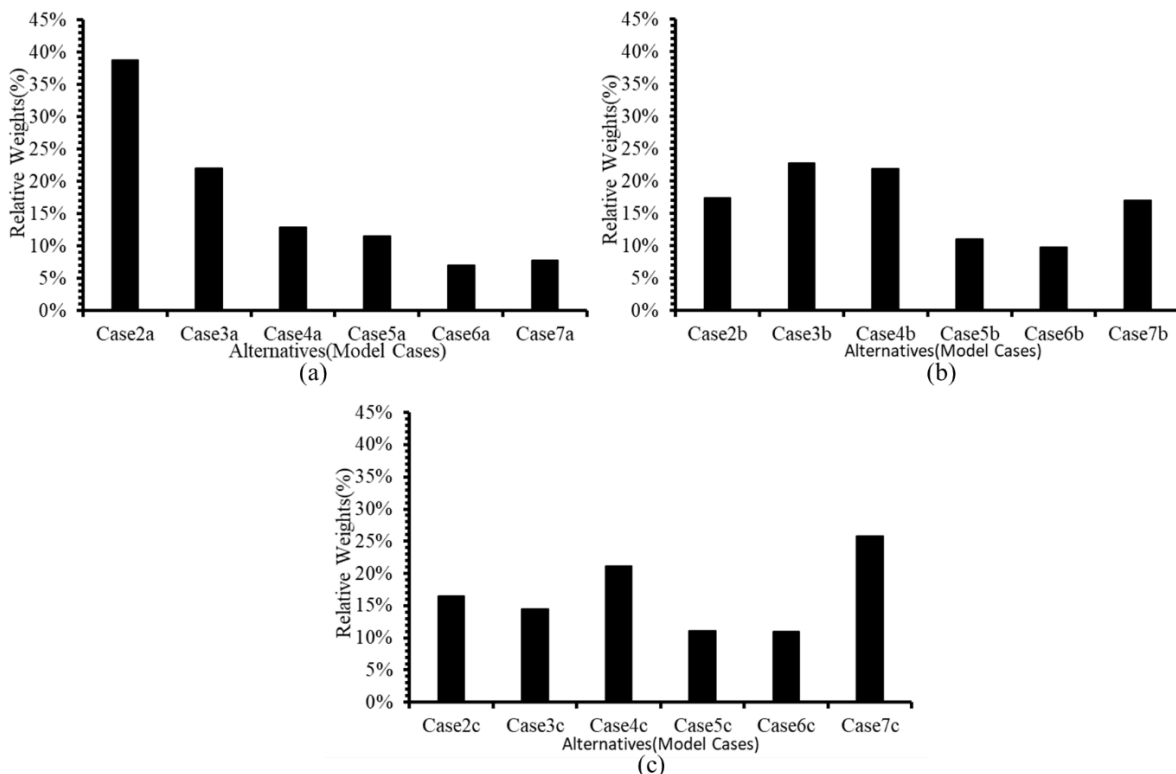
3.4.1 Level (1) Results

For the alternatives in each category, the model is applied at level (1) using the weights chosen among criteria as shown in Figure 17. According to Figure 17a, minimum HHR has the largest weight for category (a) alternatives, followed by R_r . Also, WAR has the lowest weight. Similarly, for category (b) alternatives (see Figure 17b), the same rating is observed for minimum HHR (the highest weight), followed by R_r , while WAR has the lowest weight.



523
524 **Figure 17: Level (1) criteria relative weights for different categories: (a) category (a), (b) category (b), and (c)**

525 **Figure 18** illustrates the results of the relative weights in the three categories for each alternative. It is clear that case 2a ranks
526 first in this category with a relative weight of 38.72%, then case 3a, and case 6a comes in last (see **Figure 18a**). Case 3b is the
527 best alternative in category (b), followed by Case 4b, which has a weight difference of 3.5% with Case 3b. and Case 6b is the
528 worst alternative in this category (see **Figure 18b**). Case 7c is the recommended alternative in category (c), with a weight of
529 25.83% ahead of the rest of the alternatives, followed by Case 4c, while Case 6c placed in last place in this category (see
530 **Figure 18c**).



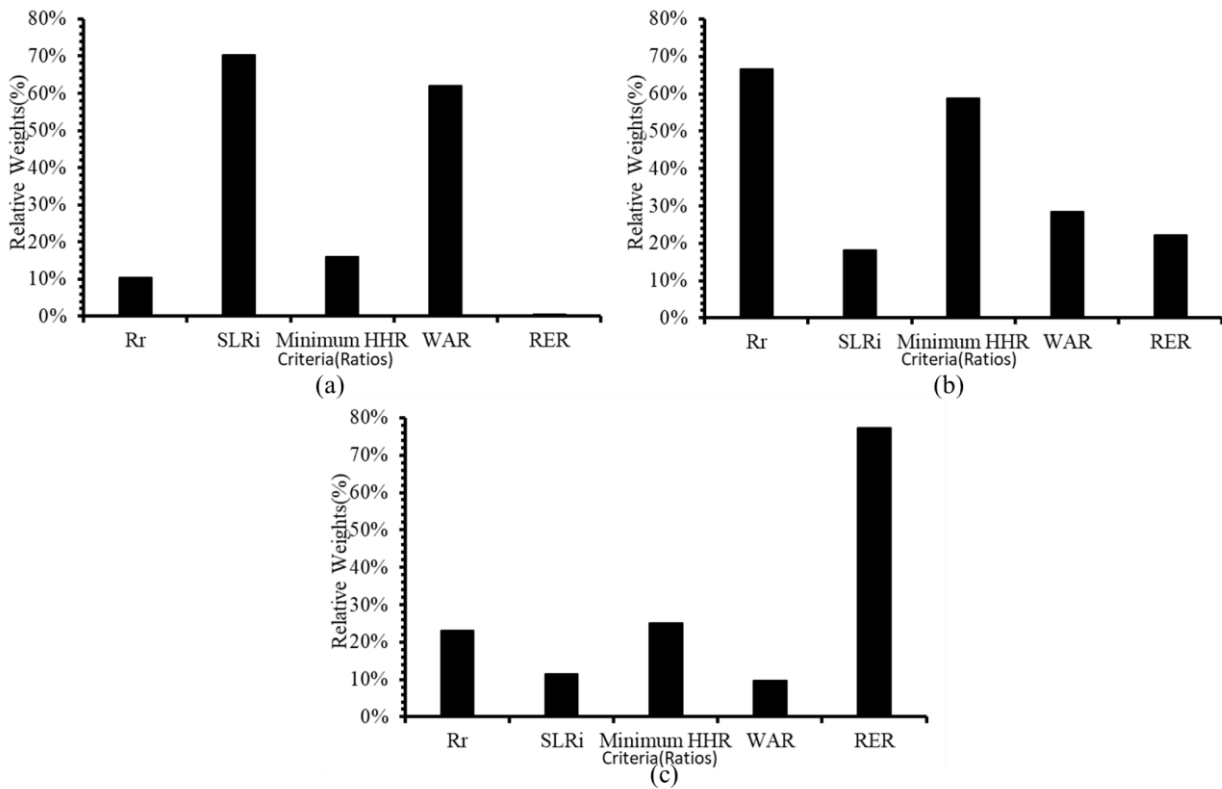
531
532 **Figure 18: Level (1) relative weights among alternatives: (a) category (a), (b) category (b), (c) category (c)**

533 3.4.2 Level (2) Results

534 The model's level (1) findings are summarized in the three best case model alternatives (cases 2a, 3b, and 7c), as shown in
535 **Figure 18**. **Figure 19** summarizes the relative weights for each criterion in relation to the three alternatives. In case 2a, SLR_i
536 is the most effective criterion, followed by WAR, while RER has a negligible effect (**Figure 19a**). On the other hand, Rr is the
537 most essential parameter influencing case 3b, followed by minimum HHR (**Figure 19b**). Case 7c is clearly influenced
538 primarily by RER (**Figure 19c**).

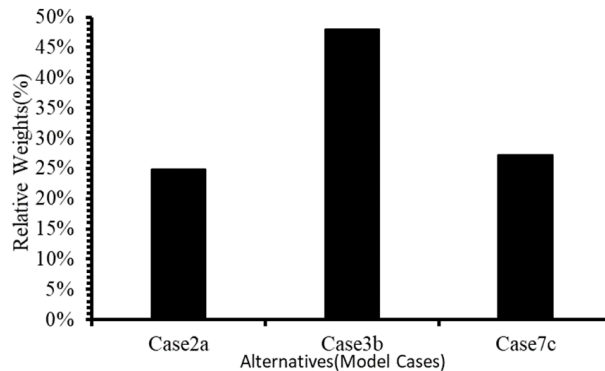
539

540



541
542 **Figure 19: Level(2) relative weights for each criterion of the alternatives for final decision: (a) case2a, (b) case3b, (c) case7c**

543 As a result of the preceding findings, **Figure 20** illustrates the weight values of the alternatives as a final decision, which
544 clearly supports Case 3b by a percentage of 47.93% over a percentage of 27.30% for Case 7c and 24.85% for Case 2a. Based
545 on the findings, it could be conclude that the components of case3b (combining the vertical barrier with surface recharge along
546 the LR ratio from 0.45 to 0.55) could be classified as best model case for use as a saltwater countermeasure. Furthermore, the
547 vertical barrier has a greater effect when combined with surface recharge than when combined with well recharge. On the
548 other hand, surface recharge necessitates a high recharge rate (about 1.25 times the borewell recharge).



549
550 **Figure 20: Level (2) relative weights for the three alternatives for final decision**

551 Conclusion

552 Seawater intrusion is a common environmental issue that degrades the quality of fresh groundwater in the coastal aquifer.
553 Because of the hydraulic connection between the coastal aquifer and the sea, using conventional physical vertical barriers
554 could reform the groundwater's hydraulic gradient, disrupt the hydrodynamic balance between the two fluids, affect the
555 potentiometric surface of the coastal aquifer, and increase saltwater intrusion. In this study, saltwater intrusion is managed by
556 controlling hydraulic heads along the coastal aquifer using surface or subsurface recharges in conjunction with the traditional
557 vertical barrier countermeasure. A physical model is created to investigate the saltwater line behavior with a vertical barrier
558 (experiment1) and without a vertical barrier (experiment2). The experimental results are used to validate a MODFLOW created

559 numerical model. Following that, three categories of model cases ((a), (b), and (c)), each with seven proposed model cases,
560 are numerically investigated for: analyzing the saltwater-freshwater interaction through porous media; selecting the best
561 location of the recharge; determining the best depth of the vertical barrier; and selecting the components of the efficient
562 countermeasure system, including the vertical barrier, surface recharge, and subsurface recharge. Evaluation ratios are
563 suggested in order to analyze and characterize the numerical model cases' saltwater line and hydraulic head variations.
564 According to category (a) simulation results, the minimum hydraulic head occurs through length ratio (LR) values ranging
565 from 0.45 to 0.55, with corresponding values of hydraulic head ratio (HHR) ranging from 0.91 to 0.98. On the other hand,
566 surface and subsurface recharge are implemented through categories (b) and (c) to investigate saltwater control by maintaining
567 the HHR value of unity within the concluded LR range. As a preset for finding the best model case, classification ratios are
568 proposed to classify the model cases included in the three mentioned categories as the best or worst model case. Using the
569 calculated classification ratio values, an analytic hierarchy process (AHP) decision-making model (DMM) is used to select the
570 best model case that is recommended for saltwater control using two selection levels. The first selection level concluded that
571 the minimum HHR has the highest relative weight in all categories, while the WAR has the lowest. Cases 2a, 3b, and 7c are
572 rated as the best model cases in categories (a), (b), and (c), respectively, and are most affected by SLR_i, R_r, and RER,
573 respectively. In the second selection level, the final decision is made that case 3b is the overall best model case, which has a
574 reasonable WAR of 1.25 and a maximum R_r of 0.29. Moreover, the findings indicate that countermeasure systems (combining
575 the vertical barrier with surface recharge) are the best choice to be used in this case.

576

577 **Data availability:** The authors support the data availability of this research, which includes experimental measurements,
578 numerical model output files, numerical model post-processed results, and AHP output results. The data source can be found
579 at <https://doi.org/10.4211/hs.8c31e2e9f8ab459ab99c61ccc110ab08> (Mahmod, 2023).

580 **Author contribution:** "Wael Elham Mahmod designed the experiments and carried them out. He also built the numerical
581 model using ModelMuse and performed the simulations and analysed the results. With contributions from all co-authors, Wael
582 Elham Mahmod prepared the manuscript. Usama Hamed Issa developed the AHP model and performed the decision-making
583 simulations.

584 **Financial Support:** This research work was funded by Institutional Fund Projects under Grant No. IFPIP-1252-137-1443
585 provided by the Ministry of Education and King Abdulaziz University, DSR, Jeddah, Saudi Arabia.

586 **Acknowledgements:** The authors gratefully acknowledge the technical and financial support provided by the Ministry of
587 Education and King Abdulaziz University, DSR, Jeddah, Saudi Arabia.

588 **Competing interests:** The contact author has declared that none of the authors has any competing interests.

589 References

590 Abarca, E., Vázquez-Suñé, E., Carrera, J., Capino, B., Gámez, D., and Batlle, F.: Optimal design of measures to correct
591 seawater intrusion, *Water Resour. Res.*, 42, <https://doi.org/10.1029/2005WR004524>, 2006.

592 Abd-Elaty, I., Abd-Elhamid, H. F., and Negm, A. M.: Investigation of Saltwater Intrusion in Coastal Aquifers, in: *Groundwater*
593 *in the Nile Delta*, edited by: Negm, A. M., Springer International Publishing, Cham, 329–353,
594 https://doi.org/10.1007/698_2017_190, 2019a.

595 Abd-Elaty, I., Abd-Elhamid, H., and Mousavi Nezhad, M.: Numerical analysis of physical barriers systems efficiency in
596 controlling saltwater intrusion in coastal aquifers, *Environ. Sci. Pollut. Res.*, 2019b.

597 Abd-Elhamid, H. F.: Investigation and control of seawater intrusion in the Eastern Nile Delta aquifer considering climate
598 change, *Water Supply*, 17, 311–323, <https://doi.org/10.2166/ws.2016.129>, 2016.

599 Abd-Elhamid, H. F. and Javadi, A. A.: A Cost-Effective Method to Control Seawater Intrusion in Coastal Aquifers, *Water*
600 *Resour. Manag.*, 25, 2755–2780, <https://doi.org/10.1007/s11269-011-9837-7>, 2011.

601 Abd-Elhamid, H. F., Abd-Elaty, I., and Negm, A. M.: Control of Saltwater Intrusion in Coastal Aquifers, in: *Groundwater in*

- 602 the Nile Delta, edited by: Negm, A. M., Springer International Publishing, Cham, 355–384,
603 https://doi.org/10.1007/698_2017_138, 2019.
- 604 Abdelwahab, S. F., Issa, U. H., and Ashour, H. M.: A Novel Vaccine Selection Decision-Making Model (VSDMM) for
605 COVID-19, *Vaccines*, 9, <https://doi.org/10.3390/vaccines9070718>, 2021.
- 606 Achu, A. L., Thomas, J., and Reghunath, R.: Multi-criteria decision analysis for delineation of groundwater potential zones in
607 a tropical river basin using remote sensing, GIS and analytical hierarchy process (AHP), *Groundw. Sustain. Dev.*, 10, 100365,
608 <https://doi.org/https://doi.org/10.1016/j.gsd.2020.100365>, 2020.
- 609 Ahmadi, H., Kaya, O. A., Babadagi, E., Savas, T., and Pekkan, E.: GIS-Based Groundwater Potentiality Mapping Using AHP
610 and FR Models in Central Antalya, Turkey, <https://doi.org/10.3390/IECG2020-08741>, 2021.
- 611 Albayrak, E. and Erensal, Y. C.: Using analytic hierarchy process (AHP) to improve human performance: An application of
612 multiple criteria decision making problem, *J. Intell. Manuf.*, 15, 491–503,
613 <https://doi.org/10.1023/B:JIMS.0000034112.00652.4c>, 2004.
- 614 Alwetaishi, M., Gadi, M., and Issa, U. H.: Reliance of building energy in various climatic regions using multi criteria, *Int. J.*
615 *Sustain. Built Environ.*, 6, 555–564, <https://doi.org/10.1016/j.ijbsbe.2017.12.002>, 2017.
- 616 Anders, R., Mendez, G. O., Futa, K., and Danskin, W. R.: A geochemical approach to determine sources and movement of
617 saline groundwater in a coastal aquifer., *Ground Water*, 52, 756–768, <https://doi.org/10.1111/gwat.12108>, 2014.
- 618 Arunbose, S., Srinivas, Y., Rajkumar, S., Nair, N. C., and Kaliraj, S.: Remote sensing, GIS and AHP techniques based
619 investigation of groundwater potential zones in the Karumeniyar river basin, Tamil Nadu, southern India, *Groundw. Sustain.*
620 *Dev.*, 14, 100586, <https://doi.org/https://doi.org/10.1016/j.gsd.2021.100586>, 2021.
- 621 ASCE: Standard Guidelines for Artificial Recharge of Ground Water, EWRI/ASCE., American Society of Civil Engineers,
622 <https://doi.org/10.1061/9780784405482>, 2001.
- 623 Bakker, M., Schaars, F., Hughes, J. D., Christian D. Langevin, A., and Dausman, A. M.: Documentation of the seawater
624 intrusion (SWI2) package for MODFLOW: U.S. Geological Survey Techniques and Methods, book 6, chap. A46, 47 p. pp.,
625 2013.
- 626 Cai, J., Taute, T., and Schneider, M.: Recommendations of Controlling Saltwater Intrusion in an Inland Aquifer for Drinking-
627 Water Supply at a Certain Waterworks Site in Berlin (Germany), *Water Resour. Manag.*, 29, 2221–2232,
628 <https://doi.org/10.1007/s11269-015-0937-7>, 2015.
- 629 Cary, L., Petelet-Giraud, E., Bertrand, G., Kloppmann, W., Aquilina, L., Martins, V., Hirata, R., Montenegro, S., Pauwels, H.,
630 Chatton, E., Franzen, M., Aurouet, A., Lasseur, E., Picot, G., Guerrot, C., Fléhoc, C., Labasque, T., Santos, J. G., Paiva, A.,
631 Braibant, G., and Pierre, D.: Origins and processes of groundwater salinization in the urban coastal aquifers of Recife
632 (Pernambuco, Brazil): A multi-isotope approach, *Sci. Total Environ.*, 530–531, 411–429,
633 <https://doi.org/https://doi.org/10.1016/j.scitotenv.2015.05.015>, 2015.
- 634 Castillo, J. L., Martínez Cruz, D. A., Ramos Leal, J. A., Tuxpan Vargas, J., Rodríguez Tapia, S. A., and Marín Celestino, A.
635 E.: Delineation of Groundwater Potential Zones (GWPZs) in a Semi-Arid Basin through Remote Sensing, GIS, and AHP
636 Approaches, <https://doi.org/10.3390/w14132138>, 2022.
- 637 Domenico, P. A., Schwartz, F. W., and SCHWARTZ, F. A.: *Physical and Chemical Hydrogeology*, Wiley, 1998.
- 638 Eissa, M. A., de Dreuzy, J.-R., and Parker, B.: Integrative management of saltwater intrusion in poorly-constrained semi-arid
639 coastal aquifer at Ras El-Hekma, Northwestern Coast, Egypt, *Groundw. Sustain. Dev.*, 6, 57–70,
640 <https://doi.org/https://doi.org/10.1016/j.gsd.2017.10.002>, 2018.
- 641 G.U.N.T: [https://www.gunt.de/en/products/hydraulics-for-civil-engineering/hydraulic-engineering/seepage-
642 flow/visualisation-of-seepage-flows/070.16900/hm169/glct-1:pa-148:ca-181:pr-768](https://www.gunt.de/en/products/hydraulics-for-civil-engineering/hydraulic-engineering/seepage-flow/visualisation-of-seepage-flows/070.16900/hm169/glct-1:pa-148:ca-181:pr-768), last access: 14 September 2023.
- 643 Gangadharan, R., Nila, R., and Vinoth, S.: Assessment of groundwater vulnerability mapping using AHP method in coastal
644 watershed of shrimp farming area, *Arab. J. Geosci.*, 9, 1–14, <https://doi.org/10.1007/s12517-015-2230-8>, 2016.
- 645 Güllü, Ö. and Kavurmacı, M.: Investigation of temporal variation of groundwater salinity potential using AHP-based index,
646 *Environ. Monit. Assess.*, 195, 365, <https://doi.org/10.1007/s10661-023-10993-5>, 2023.
- 647 Harbaugh, A. W.: MODFLOW-2005: the U.S. Geological Survey modular ground-water model--the ground-water flow
648 process, *Techniques and Methods*, <https://doi.org/10.3133/tm6A16>, 2005.
- 649 Hasan, M. B., Driessen, P. P. J., Majumder, S., Zoomers, A., and van Laerhoven, F.: Factors Affecting Consumption of Water
650 from a Newly Introduced Safe Drinking Water System: The Case of Managed Aquifer Recharge (MAR) Systems in
651 Bangladesh, <https://doi.org/10.3390/w11122459>, 2019.
- 652 Huang, P.-S. and Chiu, Y.-C.: A Simulation-Optimization Model for Seawater Intrusion Management at Pingtung Coastal

- 653 Area, Taiwan, *Water*, 10, <https://doi.org/10.3390/w10030251>, 2018.
- 654 Issa, U. H., Mosaad, S. A. A., and Salah Hassan, M.: Evaluation and selection of construction projects based on risk analysis,
655 *Structures*, 27, 361–370, <https://doi.org/https://doi.org/10.1016/j.istruc.2020.05.049>, 2020.
- 656 Kallioras, A., Pliakas, F.-K., Schüth, C., and Rausch, R.: Methods to Countermeasure the Intrusion of Seawater into Coastal
657 Aquifer Systems, in: *Wastewater Reuse and Management*, 470–490, https://doi.org/10.1007/978-94-007-4942-9_17, 2013.
- 658 M Armanuos, A., Gamal Eldin Ibrahim, M., Mahmod, W., Takemura, J., and Yoshimura, C.: Analysing the Combined Effect
659 of Barrier Wall and Freshwater Injection Countermeasures on Controlling Saltwater Intrusion in Unconfined Coastal Aquifer
660 Systems, *Water Resour. Manag.*, 33, <https://doi.org/10.1007/s11269-019-2184-9>, 2019.
- 661 Maliva, R. G.: ASR and Aquifer Recharge Using Wells, in: *Anthropogenic Aquifer Recharge: WSP Methods in Water
662 Resources Evaluation Series No. 5*, Springer International Publishing, Cham, 381–436, https://doi.org/10.1007/978-3-030-11084-0_13, 2020a.
- 664 Maliva, R. G.: Surface-Spreading AAR Systems (Non-basin), in: *Anthropogenic Aquifer Recharge: WSP Methods in Water
665 Resources Evaluation Series No. 5*, Springer International Publishing, Cham, 517–565, https://doi.org/10.1007/978-3-030-11084-0_16, 2020b.
- 667 Mallick, J., Khan, R. A., Ahmed, M., Alqadhi, S. D., Alsubih, M., Falqi, I., and Hasan, M. A.: Modeling Groundwater Potential
668 Zone in a Semi-Arid Region of Aseer Using Fuzzy-AHP and Geoinformation Techniques, <https://doi.org/10.3390/w11122656>,
669 2019.
- 670 Mantoglou, A.: Pumping management of coastal aquifers using analytical models of saltwater intrusion, *Water Resour. Res.*,
671 39, <https://doi.org/https://doi.org/10.1029/2002WR001891>, 2003.
- 672 Nithya, C. N., Srinivas, Y., Magesh, N. S., and Kaliraj, S.: Assessment of groundwater potential zones in Chittar basin,
673 Southern India using GIS based AHP technique, *Remote Sens. Appl. Soc. Environ.*, 15, 100248,
674 <https://doi.org/https://doi.org/10.1016/j.rsase.2019.100248>, 2019.
- 675 Osiakwan, G. M., Gibrilla, A., Kabo-Bah, A. T., Appiah-Adjei, E. K., and Anornu, G.: Delineation of groundwater potential
676 zones in the Central Region of Ghana using GIS and fuzzy analytic hierarchy process, *Model. Earth Syst. Environ.*, 8, 5305–
677 5326, <https://doi.org/10.1007/s40808-022-01380-z>, 2022.
- 678 Özat, S. T.: Determination of criterion that affects supplier selection in public administration software tenders and selection of
679 supplier2013 ,.
- 680 Panthi, J., Pradhanang, S. M., Nolte, A., and Boving, T. B.: Saltwater intrusion into coastal aquifers in the contiguous United
681 States — A systematic review of investigation approaches and monitoring networks, *Sci. Total Environ.*, 836, 155641,
682 <https://doi.org/https://doi.org/10.1016/j.scitotenv.2022.155641>, 2022.
- 683 Pham, Q. N., Ta, T. T., Le Tran, T., Pham, T. T., and Nguyen, T. C.: Assessment of Saltwater Intrusion Vulnerability in the
684 Coastal Aquifers in Ninh Thuan, Vietnam BT - *Global Changes and Sustainable Development in Asian Emerging Market
685 Economies Vol. 2: Proceedings of EDESUS 2019*, edited by: Nguyen, A. T. and Hens, L., Springer International Publishing,
686 Cham, 703–712, https://doi.org/10.1007/978-3-030-81443-4_45, 2022.
- 687 Phin, T. T., Hoa, D. T. B., Trong, T. D., Hai, D. T., and Que, P. T. N.: Mapping vulnerability water supply in Rach Gia city
688 due to saline intrusion on using analytical hierarchy process, *Sustain. Water Resour. Manag.*, 8, 137,
689 <https://doi.org/10.1007/s40899-022-00712-2>, 2022.
- 690 Pollock, D. W.: User guide for MODPATH Version 7—A particle-tracking model for MODFLOW, Open-File Report, Reston,
691 VA, 41 pp., <https://doi.org/10.3133/ofr20161086>, 2016.
- 692 Pramada, S. K., Minnu, K. P., and Roshni, T.: Insight into sea water intrusion due to pumping: a case study of Ernakulam
693 coast, India, *ISH J. Hydraul. Eng.*, 27, 442–451, <https://doi.org/10.1080/09715010.2018.1553642>, 2021.
- 694 Presley, A.: ERP investment analysis using the strategic alignment model, *Manag. Res. News*, 29, 273–284, 2006.
- 695 Qi, S.-Z. and Qiu, Q.-L.: Environmental hazard from saltwater intrusion in the Laizhou Gulf, Shandong Province of China,
696 *Nat. Hazards*, 56, 563–566, <https://doi.org/10.1007/s11069-010-9686-3>, 2011.
- 697 Raja Shekar, P. and Mathew, A.: Assessing groundwater potential zones and artificial recharge sites in the monsoon-fed
698 Murredu river basin, India: An integrated approach using GIS, AHP, and Fuzzy-AHP, *Groundw. Sustain. Dev.*, 23, 100994,
699 <https://doi.org/https://doi.org/10.1016/j.gsd.2023.100994>, 2023.
- 700 Ríos, I. H., Cruz-Pérez, N., Chirivella-Guerra, J. I., García-Gil, A., Rodríguez-Alcántara, J. S., Rodríguez-Martín, J.,
701 Marazuela, M. Á., and Santamarta, J. C.: Proposed recharge of island aquifer by deep wells with regenerated water in Gran
702 Canaria (Spain), *Groundw. Sustain. Dev.*, 22, 100959, <https://doi.org/https://doi.org/10.1016/j.gsd.2023.100959>, 2023.

- 703 Robinson, G., Ahmed, A. A., and Hamill, G. A.: Experimental saltwater intrusion in coastal aquifers using automated image
704 analysis: Applications to homogeneous aquifers, *J. Hydrol.*, 538, 304–313,
705 <https://doi.org/https://doi.org/10.1016/j.jhydrol.2016.04.017>, 2016.
- 706 Rotz, R.: Hydrogeologic Properties of Earth Materials and Principles of Groundwater Flow, *Groundwater*, 59,
707 <https://doi.org/10.1111/gwat.13085>, 2021.
- 708 Saaty, T. L.: Axiomatic foundation of the analytic hierarchy process, *Manag. Sci.*, 32, 841–855., 1986.
- 709 Sajil Kumar, P. J., Elango, L., and Schneider, M.: GIS and AHP Based Groundwater Potential Zones Delineation in Chennai
710 River Basin (CRB), India, *Sustainability*, 14, <https://doi.org/10.3390/su14031830>, 2022.
- 711 Salehi Shafa, N., Babazadeh, H., Aghayari, F., and Saremi, A.: Optimal utilization of groundwater resources and artificial
712 recharge system of Shahriar plain aquifer, Iran, *Phys. Chem. Earth, Parts A/B/C*, 129, 103358,
713 <https://doi.org/https://doi.org/10.1016/j.pce.2023.103358>, 2023.
- 714 Shao, Z., Huq, M. E., Cai, B., Altan, O., and Li, Y.: Integrated remote sensing and GIS approach using Fuzzy-AHP to delineate
715 and identify groundwater potential zones in semi-arid Shanxi Province, China, *Environ. Model. Softw.*, 134, 104868,
716 <https://doi.org/https://doi.org/10.1016/j.envsoft.2020.104868>, 2020.
- 717 Shi, L. and Jiao, J. J.: Seawater intrusion and coastal aquifer management in China: a review, *Environ. Earth Sci.*, 72, 2811–
718 2819, <https://doi.org/10.1007/s12665-014-3186-9>, 2014.
- 719 Singh, Murty, H. R., Gupta, S. K., and Dikshit, A. K.: Development of composite sustainability performance index for steel
720 industry, *Ecol. Indic.*, 7, 565–588, <https://doi.org/https://doi.org/10.1016/j.ecolind.2006.06.004>, 2007.
- 721 Singh, A.: Managing the environmental problem of seawater intrusion in coastal aquifers through simulation–optimization
722 modeling, *Ecol. Indic.*, 48, 498–504, <https://doi.org/https://doi.org/10.1016/j.ecolind.2014.09.011>, 2015.
- 723 Srinivasamoorthy, S. G. A.-S. G. A.-K.: Application of Geophysical and Hydrogeochemical Tracers to Investigate Salinisation
724 Sources in Nagapatinam and Karaikal Coastal Aquifers, South India, *Aquat. Procedia*, v. 4, 65–71–2015 v.4,
725 <https://doi.org/10.1016/j.aqpro.2015.02.010>, 2015.
- 726 Sutar, A. and Rotte, V.: Prevention of Saltwater Intrusion: A Laboratory-Scale Study on Electrokinetic Remediation, 389–400,
727 https://doi.org/10.1007/978-981-16-5501-2_31, 2022.
- 728 Vaidya, O. S. and Kumar, S.: Analytic hierarchy process: An overview of applications, *Eur. J. Oper. Res.*, 169, 1–29,
729 <https://doi.org/https://doi.org/10.1016/j.ejor.2004.04.028>, 2006.
- 730 Wadi, D., Wu, W., Malik, I., Fuad, A., and Thaw, M. M.: Assessment and feasibility of the potential artificial groundwater
731 recharge in semi-arid crystalline rocks context, Biteira district, Sudan, *Sci. African*, 17, e01298,
732 <https://doi.org/https://doi.org/10.1016/j.sciaf.2022.e01298>, 2022.
- 733 Yang, H., Jia, C., Li, X., Yang, F., Wang, C., and Yang, X.: Evaluation of seawater intrusion and water quality prediction in
734 Dagu River of North China based on fuzzy analytic hierarchy process exponential smoothing method, *Environ. Sci. Pollut.
735 Res.*, 29, 66160–66176, <https://doi.org/10.1007/s11356-022-19871-y>, 2022.
- 736 Zghibi, A., Mirchi, A., Msaddek, M. H., Merzougui, A., Zouhri, L., Taupin, J.-D., Chekirbane, A., Chenini, I., and Tarhouni,
737 J.: Using Analytical Hierarchy Process and Multi-Influencing Factors to Map Groundwater Recharge Zones in a Semi-Arid
738 Mediterranean Coastal Aquifer, *Water*, 12, <https://doi.org/10.3390/w12092525>, 2020.
- 739 Zhou, X., Chen, M., and Liang, C.: Optimal schemes of groundwater exploitation for prevention of seawater intrusion in the
740 Leizhou Peninsula in southern China, *Environ. Geol.*, 43, 978–985, <https://doi.org/10.1007/s00254-002-0722-9>, 2003.
- 741